THE CHEMISTRY OF EARTH, ATMOSPHERE, OCEAN, AND SPACE

ACS EARTH AND SPACE CHEMISTRY

MARCH 2024 VOLUME 8 NUMBER 3
pubs.acs.org/acsearthspacechem

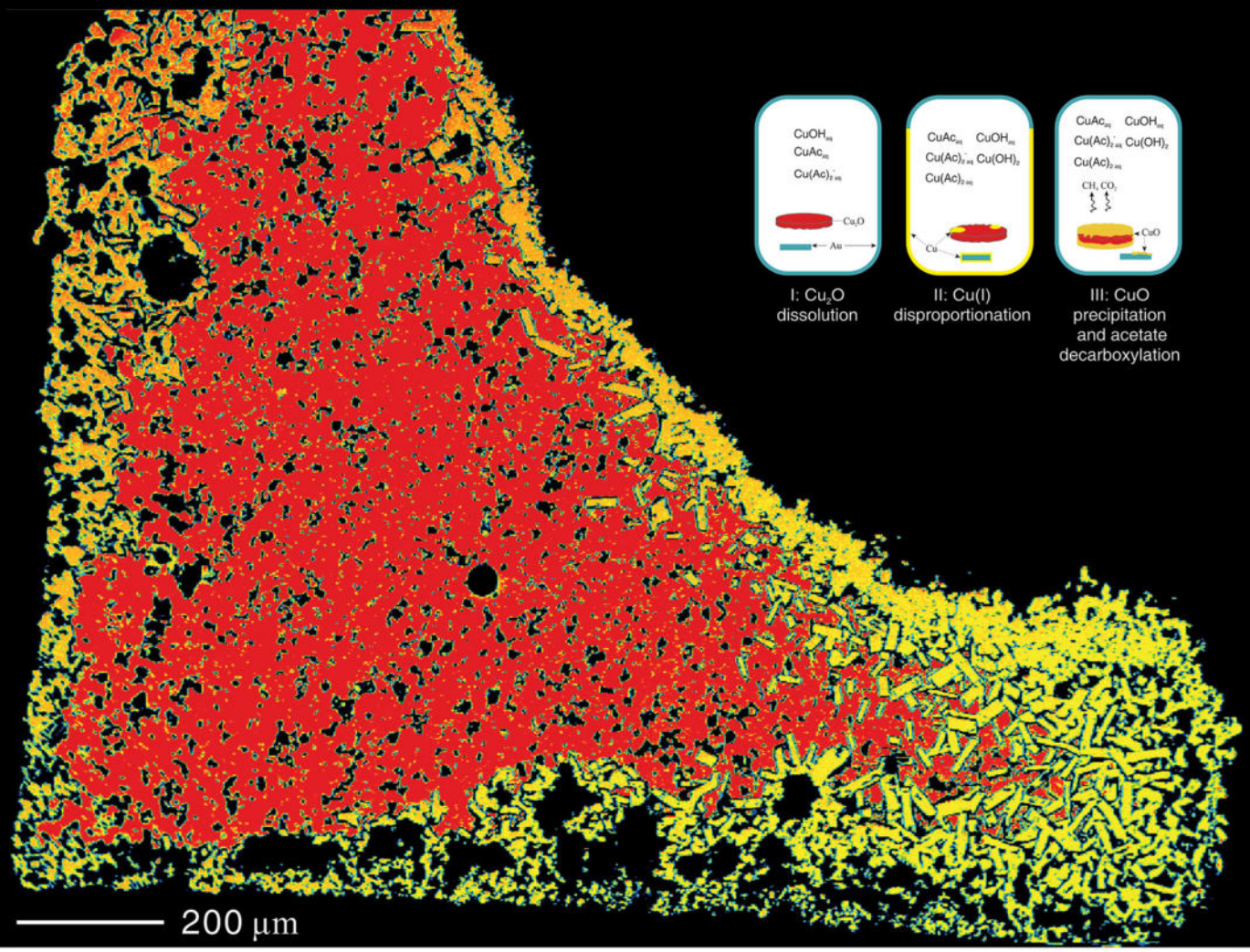

ACS Publications
Most Trusted. Most Cited. Most Read.
www.acs.org

ACS EARTH AND SPACE CHEMISTRY

Open Access

http://pubs.acs.org/journal/aesccq

Article

Experimental Study on the Reaction of Cuprite (Cu_2O) with Acetate-Bearing Hydrothermal Fluids at 100−250 °C and 5−30 MPa

Dongmei Qi,* Harald Behrens, Marina Lazarov, Roman Botcharnikov, Chao Zhang, Christian Ostertag-Henning, and Stefan Weyer

Cite This: *ACS Earth Space Chem.* 2024, 8, 499−519

Read Online

ACCESS | Metrics & More | Article Recommendations

ABSTRACT: To improve our understanding of the formation of sedimentary copper deposits, the reaction of cuprite with 0.2 m HAc-KAc or pure H_2O solutions is studied systematically at 100−250 °C and 5−30 MPa. The experiments were carried out for periods of up to 72 h in a Parr autoclave, allowing for the in situ sampling of the fluid phase. The experiments conducted in this study demonstrate that cuprite (Cu_2O) underwent a series of changes: (i) simple dissolution, (ii) Cu(I) disproportionation to native Cu and Cu(II), and (iii) subsequent oxidation into tenorite (CuO). In pure water, only (i) and (ii) steps can be discerned, whereas all three processes have been observed in an acetate-bearing system. In HAc-KAc solutions, the maximum dissolved Cu content correlates inversely with temperature, i.e., 378 to 168 μg/g at 100 and 200 °C, respectively. However, equilibrium has not been reached in our experiments and these values may be treated as minimum cuprite solubility. In situ Cu isotope analyses have been carried out by laser ablation combined with a multicollector inductively coupled plasma-mass spectrometer. The data imply that copper isotope fractionation during cuprite replacement reactions is small. Both the microscopic observations on cross sections and the analytical data support the idea that the mineral replacement reaction is controlled by a coupled dissolution-reprecipitation (CDR) mechanism. This applies to both the deposition of metallic copper and the formation of tenorite. As suggested by the formation of pore spaces in the deposited layers, only a portion of the dissolved copper is redeposited directly in situ. The isotopic analyses of the solution and solid phases show that the partial transfer of copper into the surrounding solution is not associated with a significant isotopic effect, e.g., a measured difference between Cu and Cu_2O is within 0.32 ± 0.06‰. Our study indicates that acetate plays a dual role in copper transport and deposition. On one hand, the presence of acetate strongly enhances the Cu content in solution up to 400 μg/g, implying that acetate complexation can be responsible for metal transport in hydrothermal fluids. On the other hand, decarboxylation of acetate substantially decreases the dissolved Cu and aids the precipitation of tenorite. This may lead to the co-occurrence of Cu-bearing minerals with different oxidation valence states at low temperatures in a variety of geological settings such as supergene hydrothermal systems.

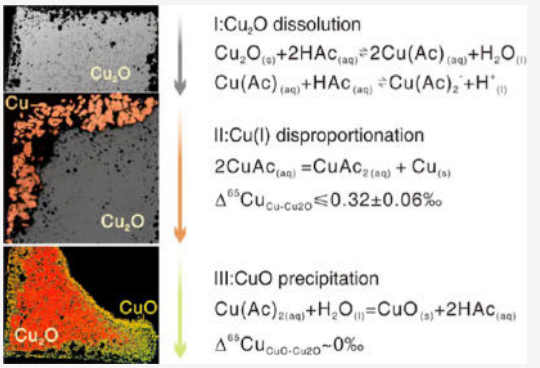

KEYWORDS: *cuprite, native copper, tenorite, coupled dissolution and reprecipitation, Cu(I) disproportion, Cu isotope fractionation, acetate*

1. INTRODUCTION

Cu transport, sequestration, and enrichment are highly dependent on its speciation in aqueous solutions, i.e., the oxidation state of copper and the formation of complexes with suitable ligands. For copper-ore settings at prevailing diagenetic conditions, at low temperatures (50−250 °C),[1] cuprous copper (Cu^+) is the predominant oxidation state, and the corresponding mineral cuprite (Cu_2O) dominates in oil field brines as well as in sediment-hosted ore deposits.[2] Modern oil field brines and basinal fluids are thought to be characteristic ore fluids responsible for the formation of sediment-hosted base metal deposits. In these fluids, chloride and bisulfide are usually thought to be the most important ligands for metal complexation. In contrast, organic agents are typically much weaker ligands. For example, a 1 M (mol/kg) sodium acetate solution at 150 °C can dissolve about 200 μg/g of copper, which is only one-third compared to a 0.1 M NaCl solution.[3,4] Nevertheless, the high abundance of organics has led to speculation as to their roles in ore-forming processes, such as acting as reaction catalyzers, reduction or oxidation medium, immobilization and mobilization of metals, and changing fluid geochemistry.[5] For

Received: September 5, 2023
Revised: December 28, 2023
Accepted: January 2, 2024
Published: January 19, 2024

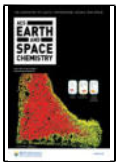

example, organics such as ketone can transport 1100 ppm Au and other platinum group elements in the Zechstein copper deposits,[6] and carboxylate ligands such as acetate play a vital role in the stabilization of metals in Mississippi Valley-type Pb−Zn deposit.[7] Moreover, acetate can also be of importance for the dissolution behavior of copper, i.e., when concentrations of halogens and bisulfide are low. Weight percent level of acetic acid and its salts are measured in oil field waters (0.5 wt %).[8,9] These fluids are not only the precursors for petroleum[10] but also are involved in the formation of sediment-hosted base metal sulfide ore deposits as well as in low-grade metamorphic ore deposits.[2,11−13] Moreover, acetate-bearing hydrothermal fluids are likely responsible for the oxidation zone development in the porphyry and/or hydrothermal Cu ore deposits.[14,15] Oxidation zones are strongly weathered and contain alteration minerals with different oxidation states, e.g., cuprite is found to coexist with native Cu and tenorite (in the most oxidized zone). The association of Cu_2O−Cu represents an intermediate replacement product.[16,17] Tenorite that replaces cuprite and native Cu is favored at alkaline or neutral pH.[17]

The stability of acetate ions (CH_3COO^-) and acetic acid (CH_3COOH) in hydrothermal fluids is of great importance for both the complex formation and oxidation state of transition metals. Hydrothermal experiments in stainless-steel vessels,[18] Ti vessels, Au cups or bags, silica tubes, and Pyrex tubes[19] have shown that aqueous solutions of acetic acid are relatively stable under thermal stress (half-lives of ca. 300−1.2×10^5 h at 350 °C). However, if suitable catalytic surfaces are present, significant decarboxylation can occur within a considerably shorter period, e.g., less than 100 h at 350 °C in the presence of magnetite or hematite.[19] Thus, the role of mineral surfaces acting either as a true catalyst, remaining unchanged, or being involved as a reactant needs to be better constrained.

Cu is a transition metal and has two stable isotopes, i.e., ^{63}Cu and ^{65}Cu. Large variations from −16.96 to 25.73‰ in Cu isotope composition have been reported in terrestrial samples,[20,21] and hence Cu isotope has been widely used to fingerprint hydrothermal activity and to uncover the processes resulting in the formation of ore bodies. Experimental calibrations demonstrate that hydrothermal processes without change in the Cu oxidation state induce Cu isotope fractionation of less than 0.70‰, e.g., fluid-rock interaction,[22] fluid-magma separation,[23] mineral dissolution,[24] and mineral precipitation processes.[25] On the other hand, redox-induced fluid−mineral interaction causes significant isotope fractionation. For example, the abiotic oxidative dissolution process can lead to aqueous Cu(II) being up to 3.1‰ heavier than its parent Cu(I) mineral.[26−32] Precipitation of Cu(I)/Cu(0) from an aqueous Cu(II) solution yields a fractionation of up to 4.0‰, with lighter Cu isotope incorporated into the reduced mineral phases.[25,33−35] Pronounced isotope fractionation occurs at low temperatures, and copper isotope fractionation up to 3‰ has been reported in sediment-hosted stratiform copper deposits.[31,36] Yet, Cu isotope fractionation between Cu(I)-bearing mineral and acetate solution has not been determined at conditions of sedimentary, metamorphic, and oxidation zone settings. Well-established experimental calibration may help to unravel the fractionation factor and controlling mechanism.

Cu is a bioessential trace metal for both humans and organisms. Biotic fractionation up to 2.5‰ has been recorded through biological uptake, sorption, redox, and organic complexation.[37−41] Copper forms stronger complexes with functional groups than abiotic forms in organic matter,[40,42] and hence complexation competes with sorption in Cu and its isotope distribution.[38,42] For instance, Cu sorption to Fe−Mn crusts is isotopically light ($\delta^{65}Cu$ of ∼0.3 to 0.5‰) compared to the residual dissolved Cu pool in seawater (∼0.9‰).[38,43] Over 99% of dissolved Cu in the ocean is organically complexed (e.g., L_1, L_2[44,45]), and organic complexation favors the heavy Cu isotope.[43,46−48] Organic complexes such as carboxyls and amines are actively involved in biological uptake induced isotope fractionation. For example, Bigalke et al.[49] reported a $\Delta^{65}Cu_{humic\text{-}Cu^{2+}}$ of 0.26 ± 0.11‰. Ryan et al.[40] measured a variable $\Delta^{65}Cu_{complex\text{-}free}$ from 0.14 to 0.84‰, where complex refers to natural and synthetic organic ligands. Thus, Cu isotopes can be used as a source and process tracer for Cu biogeochemical cycling.

This study provides information about the reaction between cuprite and acetate−acetic acid bearing fluids at the temperature of 100−250 °C and pressure of 5−30 MPa. One objective was to obtain new data on the solubility of copper in hydrothermal fluids. Furthermore, it should be tested whether significant fractionation of copper isotopes occurs during the dissolution and transformation reactions of cuprite. Another important aspect is the stability of acetate in hydrothermal systems with different types of mineral surfaces.

2. EXPERIMENTAL AND ANALYTICAL PROCEDURES

Most of the experiments and analyses were carried out at the Leibniz University of Hannover. Studies on the formation of gases during the reaction of cuprite with hydrothermal solutions were performed at the Federal Institute for Geosciences and Natural Resources (BGR) in Hannover. No unexpected or unusually high safety hazards were encountered throughout all experiments.

2.1. Reagents and Materials. As the solid starting material, sintered pellets of Cu_2O were used. This has the advantage that relicts of the starting material can be easily separated from quenched material from the fluid. The weight change of the pellet enables a first estimate of copper solubility in the fluid. Copper(I) oxide (cuprite) powder (97% purity, purchased from Sigma-Aldrich) was used to prepare the pellets. Poly(vinyl alcohol) (PVA, chemical formula $[CH_2CH(OH)]_n$) decomposes into CO_2, CO, N_2, hydrocarbons, and H_2O at 100−800 °C.[50] PVA can increase the density and the compressing strength of pellets produced, and it was added to avoid the disintegration of pellets after compaction. The preparation procedure was as follows:

(1) Mixing ∼9 g of copper(I) oxide powder, ∼2 g PVA powder, and 15 mL distilled water in a glass beaker.
(2) Stirring and cooking the mixture at 100 °C until all water has evaporated.
(3) Grinding the dry mixture into a fine powder.
(4) Compressing ca. 1 g of powder into a disc (O.D. = 13 mm, height = 1 mm) at 140 MPa.
(5) Placing pellets in a ceramic boat wrapped with a piece of copper foil to avoid any potential contaminants from the ceramic boat. To avoid the change of oxygen fugacity by PVA pyrolysis, the PVA removal is as follows. Heating at a rate of 50 °C/h to 300 °C in an atmospheric horizontal tube furnace and holding at 300 °C for 2 h to remove PVA.
(6) Adjusting the sintering conditions of Cu_2O according to Neumann et al.[51]

https://doi.org/10.1021/acsearthspacechem.3c00254
ACS Earth Space Chem. 2024, 8, 499−519

Table 1. Experimental Conditions and Formation of New Phases[a]

no.	T (°C)	P (MPa)	type of cuprite	time (h)	m_{pellet} before (g)	m_{pellet} after (g)	new phases
				Cu_2O + 0.2 m HAc/KAc			
Cp27	100	20	I	24	0.44465	0.43125	
Cp22	150	20	I	72	0.96854	n.m.	tenorite, Au−Cu
Cp26	200	20	I	24	0.49875	0.48926	
Cp29	250	5	I	24	0.42242	0.39843	native Cu
Cp30	250	10	I	24	0.66672	0.4928	native Cu
Cp43	250	20	II	6	0.14918	0.14676	
Cp24	250	20	I	72	0.96411	n.m.	tenorite, Au−Cu
Cp31	250	30	I	24	0.39616	0.38159	native Cu
Cp40	150	20	II	24	0.20402	0.19103	native Cu
	250	20		24			
	150	20		24			
				Cu_2O + H_2O			
Cp41	250	20	II	72	0.17741	n.m.	few native Cu

[a]I and II refer to type-I and type-II cuprite pellets, respectively (details are given in Section 4.3). Au−Cu indicates Au particles with a few percent of Cu. n.m. refers to not being measured. Pellets of these runs were deformed into pieces and their masses are not reliable.

(7) Cooling the ceramic boat in the air on a metal plate to ensure rapid cooling.

In the first trial, pellets were heated at 1030 °C in the air (log f_{O_2}/bar = −0.69) for 30 h. In a second attempt, pellets were heated under a CO_2 atmosphere (log f_{O_2}/bar ≈ −3, measured with a zirconia cell) at 927 °C for 24 h.

As a reference material, tenorite (CuO) pellets were prepared. Cupric oxide (CuO) powder was purchased from Johnson Matthey with a purity of 99%. CuO pellet preparation was the same as the aforementioned procedure for Cu_2O. The sintering of CuO was performed at 760 °C in the air for 24 h.

Acetic acid−acetate buffers are widely used for pH control in laboratory experiments[4,52] because of their well-defined ionization constants at elevated temperatures[53] and the relatively high threshold temperature for decarboxylation of acetate.[18,19,54] In the absence of catalytic active minerals, the decarboxylation rates of acetate at 200 and 300 °C are only 1.81 × 10^{-8} and 8.17 × 10^{-8} s^{-1}, respectively,[18] resulting in a concentration variation of less than 2% over 72 h at 300 °C.

Crystalline anhydrous potassium acetate (KAc) was purchased from Alfa Aesar, with a purity of 99%. Analytical-grade acetic acid (Ac) was acquired from Merck. Stock solutions with modal concentrations of 0.2 m (mol/kg) were prepared from both chemicals using fresh 18 mΩ, double-deionized water. The pH buffer consists of a 1:1 mixture of both solutions, yielding a pH of 4.6 determined by the pH microelectrode (described below). The pH buffer solution was used in all experiments except for Cp41 in which pure H_2O was used (details are listed in Table 2). Rubidium chloride (99.99%) powder was added to the stock solution with a concentration of ∼400 μg/g as an internal standard for mass spectrometry. This also enables monitoring of whether elements partition into different phases (vapor, liquid, and mineral) along the reaction path.

2.2. Fluid Sampling Procedure. A scheme of the reaction vessel is given in Figure 1. The setup resembles that of Dickson et al.[55] and Seyfried et al.[56] The stainless-steel autoclave (V = 250 mL; I.D. = 55 mm; O.D. = 95 mm, height = 100 mm) was purchased from Parr Instrument Company and installed with three type-J thermocouples and a manometer. The steel autoclave was filled with water and then connected to the pressure line to pressurize the system. The amount of water was adjustable by an autotuning pressure pump. To retain an inert environment, a flexible Au cell was used to separate the solution and cuprite from the pressure medium (H_2O). The reaction cell consisted of a self-made cylindrical gold cell with a star-like conic end and a volume of ∼50 mL (I.D. of 37.5 mm, O.D. of 38.3 mm, and a height of 60 mm). After loading the titanium closure and multiple runs, the Au bag is prone to deform and hence the volume will reduce to ∼30 mL (deformed Au cell in Figure 1). Deionized water was added to the reshaped cell to obtain the maximum loading of solution prior to each run. Minor air may exist and be squeezed via pressurization. Titanium parts including closure, bolts, and containers were manufactured in-house from grade 2 Ti cylinders. Ti components were passivated at 450 °C for 1 h in a 1 atm furnace prior to usage. To separate solids from fluids during sampling, a filter was installed at the end of the Ti tubing (Figure 1). The cylindrical titanium filter with a pore size of 0.5 μm, a diameter of 6.35 mm, and a height of 0.99 mm was purchased from TECHLAB, Germany. This cylinder was tightly pressed into the bore hole of a Ti cylinder and two Ti tubes were screwed in from the top and the bottom so that no liquid could flow along the side.

A piece of cuprite pellet and ∼30 mL of aqueous solution were loaded into the Au reaction cell. A small piece of gold foil (dimension of 5 × 7 mm, thickness of 0.25 mm, weight of ∼1 g) was added to identify and analyze metallic copper deposition after the run. The temperature was set by an electronic controller connected to the middle thermocouple (Figure 1). Thermocouple tips have a distance of 45 mm, and the maximum difference in temperature was less than 3 °C. The pressure was regulated by a manually controlled pump, which enabled it to build up or release pressure automatically, and the uncertainty of pressure was within 0.1 MPa. The desired pressure was adjusted before heating to check for possible leakage. During heating, the pressure was kept constant. After reaching experimental pressure and temperature, fluids could be transported through a titanium capillary tubing (Grade 5; V = 0.5 mL, I.D. = 1.60 mm, O.D. = 6.35 mm, length = 250 mm) to the titanium sampling container by opening a three-way titanium valve. A Ti connecting tube (Grade 2; V = 0.95 mL; I.D. = 5.5 mm; O.D. = 10 mm, height = 40 mm) and a Ti container (V = 0.26 mL; I.D. = 1.6 mm; O.D. = 6.35 mm, height = 13 mm) were used to temporarily sample and store in situ fluid from the Au cell.

In situ sampling of the fluid was carried out in two steps: (i) opening the first valve (Figure 1) to flush the pathways,

https://doi.org/10.1021/acsearthspacechem.3c00254
ACS Earth Space Chem. 2024, 8, 499−519

Table 2. Elements and Cu Isotope Compositions of Solutions and Solid Minerals[a]

						element concentration (μg/g)						Cu isotope composition (δ^{65}Cu, ‰)						
						Cu			Rb			solution MC-ICP-MS			in situ LA-ICP-MS			
no.	T (°C)	P (MPa)	t (h)	$pH_{ini.}$	pH_{after}	1st fl	2nd fl	res.	1st fl	2nd fl	ini.	1st fl	2nd fl	res.	dissolved Cu_2O	CuO	Cu#1	Cu#2
										Cu_2O + H_2O + pH Buffer								
Cp27	100	20	0	4.66±0.08			14			459	436		0.03±0.01					
			0.5		4.56±0.01		24			467			0.07±0.01					
			1		4.57±0.03		55			429			0.12±0.01					
			3		4.55±0.01		133			425			0.73±0.01					
			6		4.60±0.02		141			375			0.74±0.01					
			24		4.61±0.01		378	364		376			1.17±0.03	1.27±0.03	1.82±0.54			
Cp22	150	20	0	4.60±0.12		104	52		314	503	464	0.19±0.01	0.23±0.07					
			0.5		4.59±0.16	88	114		490	466		0.23±0.06	0.20±0.01					
			1			157	203		459	450		0.46±0.07	0.60±0.04					
			3			299	238		543	340		0.67±0.04	0.76±0.04					
			7			356	340		455	433		0.85±0.03	0.84±0.02					
			24			302	277		390	380		1.03±0.04	1.30±0.05					
			48		4.61±0.13	246	222		356	344		1.51±0.05	1.86±0.03					
			72		4.63±0.12	172	138	719	304	289		1.77±0.04	1.67±0.05	1.17±0.03	1.34±0.40	0.98±0.19		
Cp26	200	20	0	4.66±0.08			173			441	436		0.79±0.01					
			0.5		4.59±0.02		74			439			0.58±0.01					
			1		4.45±0.01		109			432			0.77±0.01					
			3		4.50±0.03		137			417			0.79±0.02					
			7		4.57±0.02		126			365			0.86±0.03					
			24		4.41±0.01		168	23		219			1.16±0.03	1.18±0.07	1.27±0.38			
Cp29	250	5	1	4.66±0.08	4.30±0.06		118			447	436		0.73±0.02					
			6		4.23±0.03		52			414			1.37±0.01					
			24		4.37±0.01		11	9		268			1.51±0.03	1.57±0.06	1.33±0.40		0.74±0.05	1.20±0.04
Cp30	250	10	1	4.66±0.08	4.41±0.01		86			436	436		0.53±0.03					
			6		4.33±0.04		97			426			1.04±0.01					
			24		4.37±0.05		46	23		377			1.21±0.02	1.23±0.06	1.38±0.42		0.61±0.09	1.13±0.04
Cp43	250	20	1	4.66±0.08			64			497	436		0.24±0.02					
			6		4.75±0.01		79	56		416			0.48±0.04	0.56±0.03	0.55±0.15			
Cp24	250	20	0	4.60±0.12		277	103		324	445	464	0.86±0.02	0.83±0.01					
			0.5			98	163		452	456		0.75±0.04	0.75±0.03					
			1		4.67±0.11	93	97		449	446		0.81±0.03	0.84±0.04					
			3			77	73		418	414		1.09±0.07	1.04±0.05					
			7			66	72		404	403		1.12±0.04	1.21±0.02					
			24			49	53		376	362		1.07±0.04	1.21±0.07					
			48		4.66±0.14	50	47		359	337		0.83±0.02	1.17±0.03					
			72		4.68±0.14	28	44	279	303	292		0.88±0.06	1.02±0.03	1.25±0.06	1.43±0.43	1.05±0.08		
Cp31	250	30	1	4.66±0.08	4.31±0.01		80			426	436		0.78±0.02					
			6		4.18±0.07		79			440			1.27±0.02					
			24		4.38±0.03		53	20		402			1.58±0.01	1.23±0.05	1.60±0.48		n.m.	1.30±0.04

https://doi.org/10.1021/acsearthspacechem.3c00254
ACS Earth Space Chem. 2024, 8, 499−519

Table 2. continued

						element concentration (μg/g)						Cu isotope composition (δ^{65}Cu, ‰)						
						Cu			Rb			solution MC-ICP-MS			in situ LA-ICP-MS			
no.	T (°C)	P (MPa)	t (h)	$pH_{ini.}$	pH_{after}	1st fl	2nd fl	res.	1st fl	2nd fl	ini.	1st fl	2nd fl	res.	dissolved Cu_2O	CuO	Cu#1	Cu#2
										Cu_2O + H_2O + pH Buffer								
Cp40	150	20	1	4.66±0.08	4.77±0.04		51			456	485		0.07±0.01					
			6		4.74±0.01		92			480			0.17±0.02					
			24				59			499			0.26±0.01					
	250		25		4.71±0.08		87			498			0.38±0.04					
			31		4.79±0.04		58			492			0.47±0.04					
			49				53			383			0.92±0.01					
	150		50		4.85±0.04		37			332			0.94±0.01					
			56				33			344			0.25±0.03					
			74		4.82±0.04		9.7	31		323			−0.05±0.04	0.75±0.02	0.29±0.08		0.12±0.01	0.32±0.04
										Cu_2O + H_2O								
Cp41	250	20	1	4.53±0.04	6.28±0.12		3.3			556	516		−0.23±0.01					
			12		6.57±0.04		2.9			569			0.51±0.11					
			72		7.49±0.13		1.3	1.7		459			0.46±0.03	0.06±0.03	0.44±0.12		n.m.	0.46±0.04

[a]Abbreviations: 1st fl and 2nd fluid for the first and second sampled fluids (at once), ini. and res. for an initial stock solution and residual fluid in Au reaction cell, respectively. N.M. means sample not measured. pH values of fluids are measured at room temperature for both stock and sampled solutions during the run. Except for Cp22 and Cp24, 1st flushed fluids were usually used for pH determination. pH uncertainty is the 95% confidence limit of the mean. The uncertainties of element concentrations determined by ICP-OES are better than 10% (2SD). Solution MC-ICP-MS analyses include 1st, 2nd, and res. samples solution, and in situ LA-ICP-MS measurements were performed for dissolved Cu_2O, CuO, Cu#1, and Cu#2. The uncertainties of Cu isotope data acquired by these measurements are given by the 2σ errors of the triplicated analyses. The methodological error based on repeated measurements of standards is less than 0.06‰. Cu#1 and Cu#2 refer to analyses of native copper at the cuprite pellet and on separate Au foils, respectively. Note that the listed Cu isotope compositions of CuO, Cu#1, and Cu#2 are the average values and their standard deviations; more details are given in the text.

https://doi.org/10.1021/acsearthspacechem.3c00254
ACS Earth Space Chem. 2024, 8, 499−519

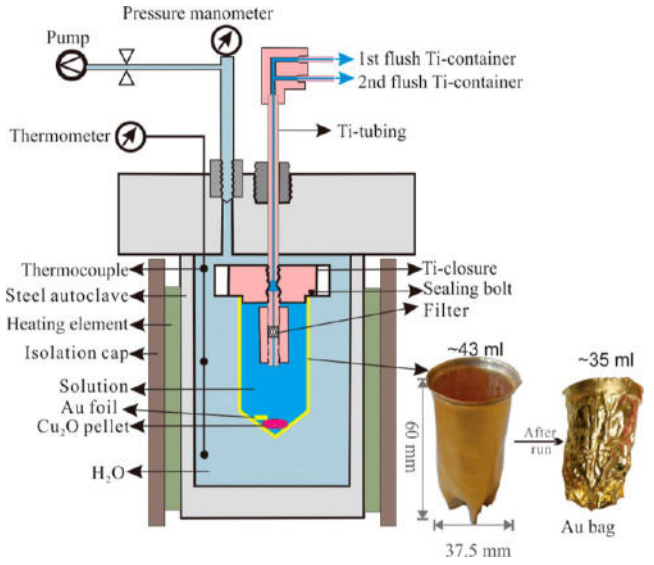

Figure 1. Schematic drawing of the fluid reactor and photo of the flexible Au cell used in the experiments (modified with permission from ref 57. Copyright 2023 Mineralogical Society of America). ~43 and ~35 mL refer to the maximum solution loaded to the Au cell with a Ti closure.

collecting the flushed liquid in a titanium container, and closing this valve immediately; (ii) opening the second valve (Figure 1) to collect the experimental fluids in the second container and closing this valve. In some cases, a third solution was taken. For doing so, the valve was immediately cooled by an air stream, and the second container was replaced by a new one. The small change in the total fluid mass (i.e., 1 g per sample compared to ~30 g of total solution loaded in the Au reaction cell) by sampling results in an instant pressure decrease of ~3 MPa in the autoclave, which was automatically compensated by the pressure pump within few seconds. The sampling containers were cooled with a compressed air gun for 10−20 min. The obtained liquids (except for the liquid for pH measurements) were transferred into Teflon vials and processed immediately with 1 mL of 1 mol/L HCl and 1 mL of deionized water to avoid possible precipitation. After cooling the autoclave and releasing the pressure, the residual liquid was transferred into a Teflon vial, and the solids were collected. The volume of the Au reaction cell after the run was less than 35 mL due to online sampling, and the Au reaction cell was rinsed with ~35 mL of 1 mol/L HCl and ~35 mL of deionized water. These collected solutions were further digested and processed with freshly prepared aqua regia solution. Potential solids retained in the rinsing solution were removed by centrifugation. The solids, such as cuprite pellet and Au foil, were dried in air and weighed again. The Au cell was cleaned with 6 mol/L HCl at 60 °C for 24 h and rinsed with water.

After each run, the deformed Au reaction cell was annealed at 850 °C for 15 min and reshaped manually. This procedure was usually repeated several times until the cylindrical shape was re-established. The inner surface of titanium containers was carefully checked for possible corrosion under a microscope. When necessary, the containers were immersed in 10% HNO_3 for 4 h at 180 °C, and the Ti passivation procedure described above was repeated.

Table 1 lists the details of each experiment. Ten experiments were performed to study the interaction of cuprite with hydrothermal fluids, i.e., the effects of run duration (24 to 72 h), temperature (100−250 °C), pressure (5−30 MPa), and pH buffer (±0.2 m HAc/KAc). To check the possible effects of pretreatment and the reversibility of the reaction, we conducted one cycling experiment (150−250−150 °C) at 20 MPa (Cp40). First, starting materials were reacted at 150 °C, and three fluid samples were collected at 1, 6, and 24 h. Then, the temperature was regulated to 250 °C and, finally, it was set back to 150 °C. After changing the temperature, conditions were accomplished within 1 h. The timing of fluid extraction at the second and third stages was similar to the first one.

2.3. Tests for Gas Production. Two experiments were performed to check for possible gas phases produced by the thermal decomposition of acetic acid. Au capsules (4.00 mm I.D., 4.40 mm O.D., and 40 mm length) were loaded with 4.5 mg of cuprite pellet and 300 mg of either pure H_2O or 0.2 m HAc/KAc solution and welded shut under a gentle gas stream of argon to enclose the fluid and solid. The mineral/fluid ratio was similar to the runs conducted in the Au reaction cell, i.e., 0.015 (mineral/fluid by mass). The experiments were performed in a stainless autoclave at 250 °C, 20 MPa for 72 h.

3. ANALYTICAL PROCEDURES

3.1. Analyses of Starting Materials and Run Products. Crystalline phases in sintered pellets were studied by X-ray powder diffraction (XRD) on a Philips PW-1800 powder diffractometer using Cu Kα radiation in steps of 0.02° between 5 and 85°. The WinXPow software (STOE) and the powder diffraction file were applied for data evaluation.

The retrieved cuprite pellet was cut through the center by a low-speed saw with a fine blade with embedded diamond powder. Half of its cross section was mounted in epoxy to prepare a thin section. Scanning electron microscopy (JEOL JSM-6390A SEM) coupled with an energy-dispersive X-ray analysis system (Bruker Quantax 200 EDXS) was employed to check the homogeneity of solids and to identify unknown phases. The acceleration voltage was set to 30.0 kV. The beam size was 1−2 μm, and the sample current was adjusted between 10 and 15 nA. The composition of cuprite and the corresponding solid products was determined using a Cameca SX 100 electron probe microanalyzer (EPMA). Standards include native metals (Cu and Au) and synthetic NaCl (Cl). A beam current of 15 nA and an acceleration voltage of 15 kV were used for all analyses. Raw data were corrected using the standard "PAP" procedure.[58]

A confocal Bruker Senterra micro-Raman spectrometer was used to identify new solid phases. It is equipped with an Olympus BX 51 microscope with a magnification objective of 50×. The spectra were collected using the 532 nm laser excitation line and recorded for 10 s with 2 times acquisition repetitions.

The pH values of some solutions were measured with an InLab Flex-Micro pH combination electrode (Mettler Toledo GmbH, Germany). All other solutions were evaporated to dryness on a 90 °C hot plate and redissolved in 1 mL of 3% HNO_3.

3.2. Element and Cu Isotope Analysis. Elemental concentrations of sampled solutions were determined by inductively coupled plasma-optical emission spectrometry (ICP-OES) on a Varian 715-ES spectrometer (Varian GmbH, Germany) equipped with a patented VistaChip CCD simultaneous detector. The samples were introduced in a concentric nebulizer and a cyclonic spray chamber. Analyses were conducted on an aliquot of ~0.5 mL (about half of the previous

https://doi.org/10.1021/acsearthspacechem.3c00254
ACS Earth Space Chem. 2024, 8, 499−519

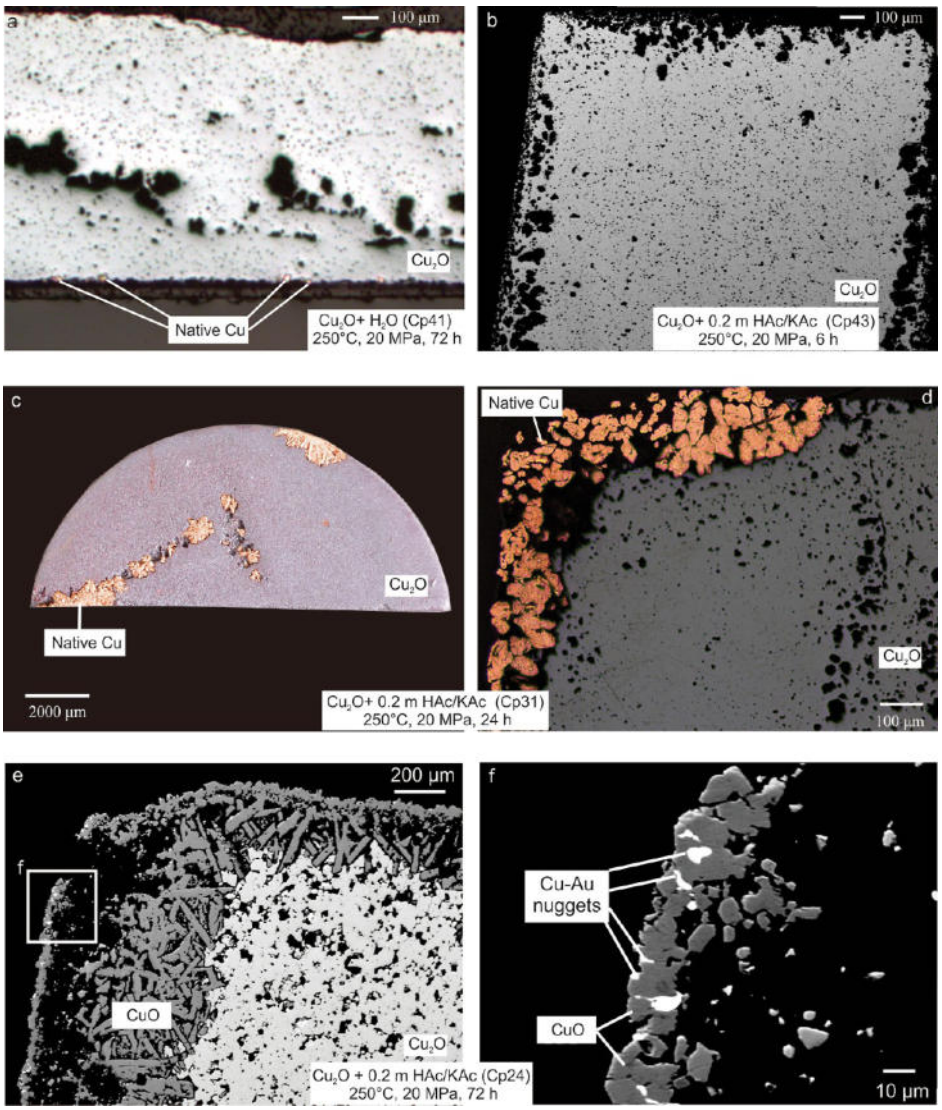

Figure 2. Images of reacted cuprite pellets in H_2O (a) and 0.2 m HAc-KAc solutions (b−f) at 250 °C. (a) Microscope image of a cross section of a retrieved cuprite pellet after 72 h at 20 MPa in H_2O. Few native copper precipitates were found at the rim of the cuprite pellet. (b) Backscattered electron image of a cuprite cross section after 6 h. No precipitates can be found. Pronounced voids near the rim developed already during the sintering of the pellet. (c) Photograph of a reacted cuprite surface. (d) Microscopic image of the cross section of the cuprite pellet shown in (c). Native copper has been observed at the rim and in open voids of the cuprite pellet. (e,f) BSE images of the cuprite cross section after 72 h. (f) Details showing Au−Cu particles within the tenorite layer.

redissolved solution) that was diluted with 3% HNO_3 to 6−11 mL. A standard solution containing seven elements (Na, K, Ti, Fe, Ni, Cu, and Rb) in concentrations of 1, 5, 10, 30, and 50 μg/g was used for calibration. In the following text, C_{Cu} refers to Cu content. All solution analyses followed the procedure reported by Roebbert et al.[59]

The Cu isotope composition of solutions and solid minerals was determined by a Thermo Scientific Neptune multicollector inductively coupled plasma-mass spectrometer. For in situ isotope measurements on solids, the MC-ICP-MS was coupled to a deep UV femtosecond laser ablation system (UV-fsLA-MC-ICP-MS).[41,42] A quartz glass spray chamber (double pass of Scott design) and a PFA microflow nebulizer (uptake rate ∼100 μL/min) were used to aspirate standard (Ni NIST SRM 986) and sample solutions. Pt or Al skimmer cones were employed, and a low-mass-resolution mode has been used for Cu isotope measurements. Masses of isotopes ^{60}Ni, ^{61}Ni, ^{62}Ni, ^{63}Cu, ^{64}Ni, and ^{65}Cu were detected simultaneously. A NIST SRM 976 standard solution and NIST SRM 976 Cu metal were used for standard-sample-standard bracketing, usually with 2−3 samples run between two standards.[60]

The analytical procedures for Cu isotope measurements at LUH have been described in detail by Lazarov and Horn.[61] For solution nebulization MC-ICP-MS analyses, the remaining half of the redissolved sample solution was diluted with 3% HNO_3 to a Cu concentration of ∼0.5 μg/g, based on previous Cu concentration data, and doped with 1 μg/g Ni NIST SRM 986 standard solution that was used to monitor instrumental mass bias. The internal uncertainty of individual measurements and the daily reproducibility of the standard and samples were better than 0.03‰ (2SE) and 0.06‰ (2SD), respectively. For solids analyzed with UV-fs LA-MC-ICP-MS, two chalcopyrite in-house standards (cpy1 and cpy2, previously characterized by Lazarov and Horn[61]) were measured as secondary standards to verify that the laser energy was set to the appropriate level and as a measure for the accuracy of the LA-MC-ICP-MS analyses (i.e.,

https://doi.org/10.1021/acsearthspacechem.3c00254
ACS Earth Space Chem. 2024, 8, 499−519

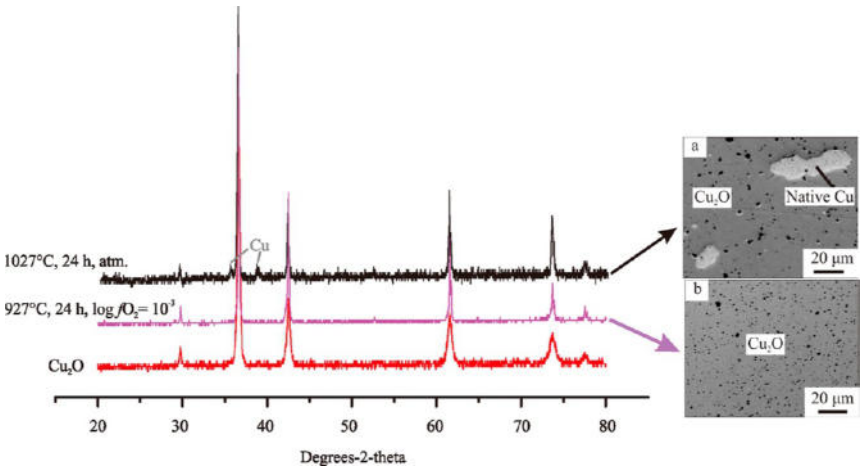

Figure 3. XRD analyses of the used cuprite powder (red) in comparison to synthesized cuprite pellets (black and purple). (a) Cuprite and copper were sintered at 1030 °C, atmosphere condition, for 24 h. (b) Cuprite pellet was sintered at 927 °C, $\log f_{O_2}/\text{bar} = 10^{-3}$ and 24 h. According to the RRUFF database (Raman spectroscopy, X-ray diffraction and chemistry of minerals), cuprite (R140763) shows peaks at 29, 36, 42, 61, and 73 and copper (R061078) at 35 and 38 (2θ).

to ensure that the analyzed values are consistent with those previously determined by solution MC-ICP-MS analyses[61]). Reference materials and samples (excluding Au foils) were ablated along lines (to avoid potential depth effects during laser ablation). The Au foils covered by thin Cu layers were analyzed by a raster pattern. A spot diameter of 40 μm and laser repetition rates of 5 and 10 Hz for NIST SRM 976 and cpy1, 2, respectively, resulted in ion beams of $\sim 1.5 \times 10^{-10}$ A (corresponding to ~15 V on 10^{11} Ω amplifiers) on mass 65 (^{65}Cu). To achieve a similar ion beam, ^{65}Cu cuprite pellets, tenorite, and native Cu crystals on cuprite and Au foil were adjusted with a repetition rate of 5−7, 2, 6−10, and 2−12 Hz, respectively. The overall double relative standard error (2SE) for samples was less than 0.04‰, similar to that reported by Lazarov and Horn.[61] Copper isotopic data are reported in standard δ notation in per mil relative to the international reference material SRM NIST 976

$$\delta^{65}\text{Cu}\ (‰) = ([((^{65}\text{Cu}/^{63}\text{Cu})_{\text{sample}}/(^{65}\text{Cu}/^{63}\text{Cu})_{\text{NIST 976}}) - 1] \times 1000) \quad (1)$$

3.3. Analyses of Gases by Gas Chromatographic Methods. For the experiments in the closed gold capsules (cf. chap. 2.3), the gas composition after the experiment was determined. The gold capsules were cleaned after the experiment with consecutive rinses of water, methanol, and dichloromethane. Afterward, the outer surface was dried with a stream of nitrogen gas. Then, the gold capsule was loaded in a 22 mL headspace vial that was capped with a septum. Through the septum, the gas phase in the headspace vial was purged with nitrogen to remove the atmosphere for 10 min. Then, the gold capsules were pierced through the septum to release the fluids and gases into the headspace vial. The release gases were identified and quantified using a modified refinery gas analyzer.[62]

4. RESULTS

4.1. Solid Phases. Relict cuprite and newly formed tenorite (CuO), Au−Cu nuggets, and native Cu were found in the run products, depending on run conditions (i.e., run duration and temperature; Table 1). The term Au−Cu nuggets refers to small metallic particles. Electron microprobe analyses of these particles yield compositions of ≈97 wt % Au and ≈3 wt % Cu (Table 1).

In the Cu_2O-H_2O system, one experiment (Cp41) was performed at 250 °C and 20 MPa for 72 h. Very few particles of native copper were deposited at the rim of the cuprite pellet and on the surface of the Au foil (Figure 2a).

In the Cu_2O-0.2 m HAc/KAc system, 9 experiments were performed at 100−250 °C and 5−30 MPa. At 100 °C, only the relict cuprite was retrieved after 24 h (similar to Figure 2b), but no new phases were formed. At 150 °C, cuprite, tenorite, and a few Au−Cu particles were observed after 72 h (similar to Figure 2e,f). The thickness of the tenorite layer around the pellet varies between 40 and 300 μm. At 200 °C, cuprite was the only solid phase retrieved after 24 h (similar to Figure 2b). At 250 °C, a series of comparable experiments were conducted with a duration of 6 to 72 h. (i) After 6 h, only cuprite residue was found (Figure 2b). (ii) After 24 h, massive native Cu precipitates occurred at the outer rim of the cuprite (denoted as Cu#1) and on the surface of the Au substrate (denoted as Cu#2). Cu#1 was heterogeneously distributed and locally replaced by Cu_2O, i.e., the basic shape of the pellet was preserved (Figures 2c and 6). Cu#1 has a grain size ranging from 20 to 100 μm (Figure 2d). It is worth noting that pressure variation from 5 to 30 MPa does not noticeably affect Cu#1 precipitation. Cu#2 precipitates were uniformly formed all over the gold surfaces and not only near the cuprite pellet, indicating that the deposition occurred from the solution. The mass gain of the added Au foils indicates a maximum thickness of the deposited Cu#2 layer on Au substrates less than 2 μm. (iii) After 72 h, tenorite crystals, and a few metallic particles were found (Figure 3e,f). A layer (~200 μm) of tenorite has been generated around the cuprite pellet (Figure 3e). The outer rim consists of fine-grained tenorite and prismatic tenorite crystal intergrowths into the cuprite. Rarely, tenorite crystals were found in voids within the cuprite polycrystal. The small piece of Au foil retrieved after the run was also covered by a dark layer of tenorite (identified by Raman spectroscopy). Au−Cu particles were observed only near the outer tenorite rim on one side of the pellet. Most likely, these particles are abrasions of the gold cells, which were trapped in the growing tenorite layer. It is worth noting that the amount of

https://doi.org/10.1021/acsearthspacechem.3c00254
ACS Earth Space Chem. 2024, 8, 499−519

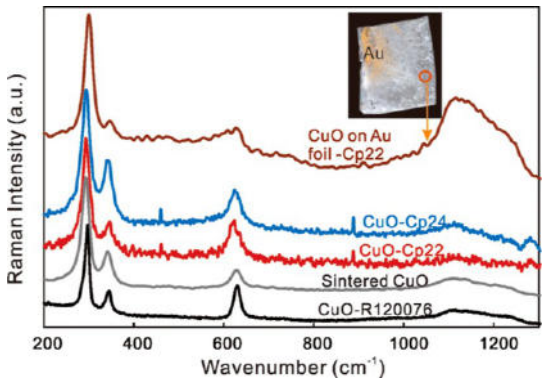

Figure 4. Raman spectra of newly formed tenorite in experiments Cp22 and Cp24 compared to the self-made tenorite reference (sintered CuO) and a synthetic tenorite from the RRUFF database (https://rruff.info/tenorite/display=default/R120076). Spectra are scaled to the same peak height at ~296 cm^{-1} for comparison.

these nuggets and their copper content are very small in Cp22 and Cp24 runs compared to the native copper precipitation in the other high-temperature experiments.

4.2. Determination of Solid Phases. Sintered cuprite pellets have been analyzed using XRD. In addition to the dominant features of Cu_2O, peaks of native Cu were observed in the pellet sintered at atmospheric conditions at 1030 °C. BSE images show that the Cu particles can have a size of several tens of micrometers (Figure 3a). We attribute these findings to an imprecision of the phase diagram of Cu−O published in Neumann et al.,[51] i.e., the conditions were too close to the boundaries of the stability field of Cu_2O. On the other hand, the cuprite pellet sintered at reduced conditions, but it turned out to be pure and chemically homogeneous at lower temperatures (Figure 3b). Large pores in the edge regions of the pellets are conspicuous for both intact and reacted Cu_2O, which were attributed to the evaporation of copper species during sintering as well as mass loss into the solution (e.g., Figure 2b). These conditions (927 °C, 24 h, $\log f_{O_2}/\mathrm{bar} = 10^{-3}$) were selected for sintering of the starting materials.

The Raman spectra of newly formed crystalline phases surrounding cuprite (e.g., Figure 2e) and dark solids from the retrieved Au foil of Cp22 are shown in Figure 4. These spectra, a self-made CuO pellet and a tenorite reference from RRUFF database, are compared. The results give clear evidence that tenorite has been formed both on cuprite and on Au foil in Cp22 and Cp24 with typical peaks at 291, 338, and 633 cm^{-1} and a broad peak of 1110−1420 cm^{-1}.

4.3. Cu Isotope Composition of Solids. *4.3.1. Cuprite (Cu_2O).* Cu_2O sintering is carried out in a gas furnace with flowing CO_2 at 1030 °C, and this leads to isotopically light cores (0‰) and heavy rims (~1.7‰). This effect was more pronounced for the upper side of the pellet, which was in direct contact with the gas phase, than for the bottom side placed on a copper foil (e.g., Figures 5 and 6). This kinetic process is driven by the evaporation as well as the diffusion of Cu isotopes in gas, which leads to the progressive enrichment of its heavier isotope in the residue Cu_2O. Such isotopic fractionation during evaporation and diffusion has been documented in other materials as well—for example, the evaporation of copper from molten basaltic glass in argon induces a Cu isotope fractionation by ~18‰.[63]

A crucial point for the analysis of copper isotope fractionation is the determination of the precise δ^{65}Cu of the dissolved cuprite (Table 2). In the first experiments, we used the type-I cuprite pellets as received after sintering (Tables 1, 2 and Figure 5). Surficial areas are full of pores and a rough estimation indicates a porosity of ~30%. Line scans with UV-fs LA-MC-ICP-MS give clear evidence for a strong enrichment of ^{65}Cu at both basal planes, where δ^{65}Cu of up to ~1.65‰ for the top side and up to 1.11‰ for the bottom side were measured near the edges (Figure 5). On the other hand, the lateral side of the pellets seems to be less influenced by copper evaporation and isotopic enrichment with measured δ^{65}Cu of ~0.2‰ near the edge. For these experiments, only a rough estimate of the effective δ^{65}Cu

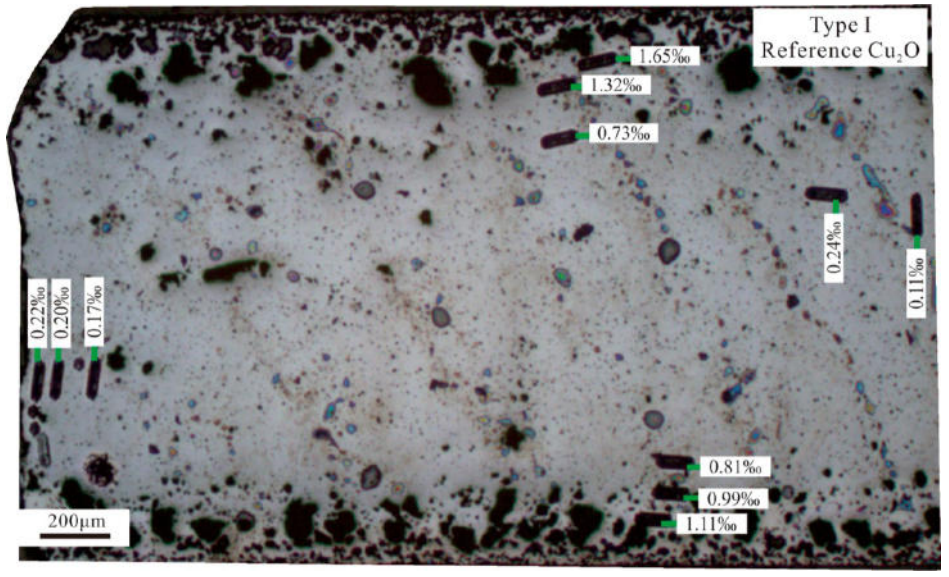

Figure 5. Microscope picture of a cross section of a sintered type-I cuprite pellet (Cp0). Thick black lines marked with green bars represent laser ablation measurements and the numbers next to them are the measured δ^{65}Cu values. Porous regions near the basal planes were formed by the evaporation of copper during sintering at high temperature. Note the difference in copper isotopic composition near the basal planes and the side planes.

https://doi.org/10.1021/acsearthspacechem.3c00254
ACS Earth Space Chem. 2024, 8, 499−519

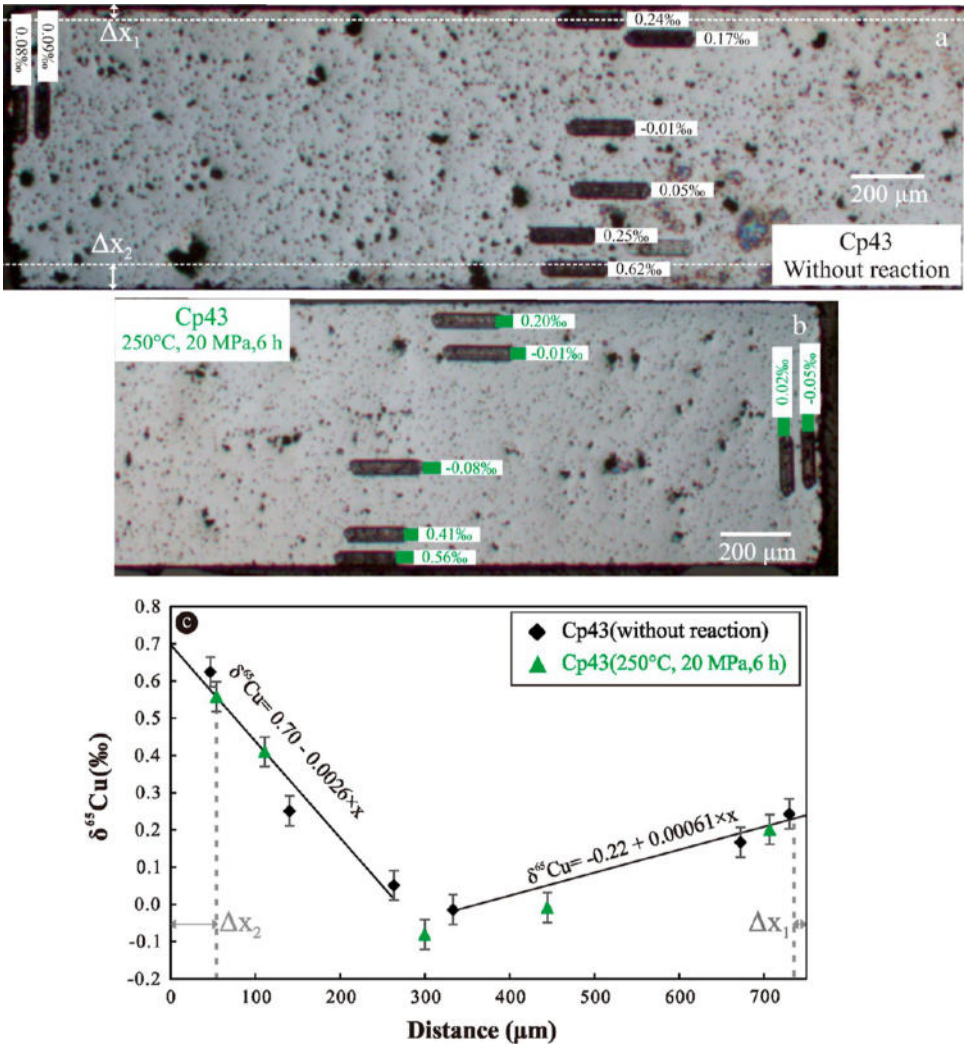

Figure 6. (a,b) Cross section of type-II cuprite pellets of Cp43 before (a) and after the (b) reaction with an acetic solution. Thick black lines are laser-ablated lines, and Cu isotope compositions of the removed materials are given next to them. White dashed lines in the reference sample (a), labeled with Δx_1 and Δx_2, mark the respective positions of the edges after the reaction, i.e., the sample surface in (b). (c) Corresponding δ^{65}Cu values of cuprite as a function of distance from the initial lower basal plane. The calculated δ^{65}Cu value of the dissolved cuprite is 0.55 ± 0.15‰. Run Cp43 was carried out in 0.2 m HAc-KAc solution at 250 °C, 20 MPa for 6 h.

of the dissolved material is possible based on the postexperimental LA-MC-ICP-MS measurements and comparison to the reference sample (one intact pellet). Linear regressions of all analyses of type-I pellets indicate that the evaporation effect on the Cu isotope gradient is weaker in the core zone of ~300 μm (approaches 0‰), which is about 650 and 500 μm to the rims (Figure 5). However, a Cu_2O pellet with a thickness of 300 μm is too thin to be fully retrieved after periodical fluid extraction and the subsequent Au bag deformation. The removal of 200 μm from both major surfaces is to remove the highly porous outer region (Figures 5 and 6a) and to retrieve the solid entirely. These polished pellets (type-II Cu_2O) yield δ^{65}Cu of ~0.6 to ~0‰ of the long rims and are the same as those of short rims of type-I Cu_2O. Type-II pellets were cut into two pieces, one of which was kept as a reference for later analysis, and the other one was used in the experiments (Cp40-Cp43, Figure 6a,b and Table 2). On the one hand, the Cu_2O dissolution front proceeds within 50 μm from the rim based on the maximum dissolved Cu in Table 2. On the other hand, copper diffusion in cuprite leads to a diffusion layer of 10.04 μm at 100−250 °C for 72 h.[64] The isotopic profiles remain invariant at 100−250 °C and 72 h, and hence, the δ^{65}Cu of the reacted Cu_2O can be estimated precisely by comparing the intact and dissolved Cu_2O.

The determination of the δ^{65}Cu values of the dissolved cuprite for type-II pellets is illustrated in Figure 6. Data of the reacted cuprite and the reference sample plot well on straight lines (Figure 6c). The reference cuprite was used to derive linear relationships $\delta^{65}\text{Cu} = a + b\cdot\Delta x$, where a and b are fitting parameters, and Δx is the distance to the original surface of the pellet. Isotopic data of the reacted pellet half (Figure 6b) and the reference piece (Figure 6a) are consistent, confirming that copper isotopes remain unfractionated by diffusion at the temperatures of the conducted experiments.

Based on the linear relationships, the average δ^{65}Cu of the dissolved layers was calculated ($\delta 1$ and $\delta 2$, respectively). After weight determination using the thickness of the dissolved layers, the isotope composition of the dissolved material can be determined as

$$\delta^{65}\text{Cu (‰)} = \delta 1 \times \frac{\Delta x_1}{\Delta x_1 + \Delta x_2} + \delta 2 \times \frac{\Delta x_2}{\Delta x_1 + \Delta x_2} \quad (2)$$

https://doi.org/10.1021/acsearthspacechem.3c00254
ACS Earth Space Chem. 2024, 8, 499−519

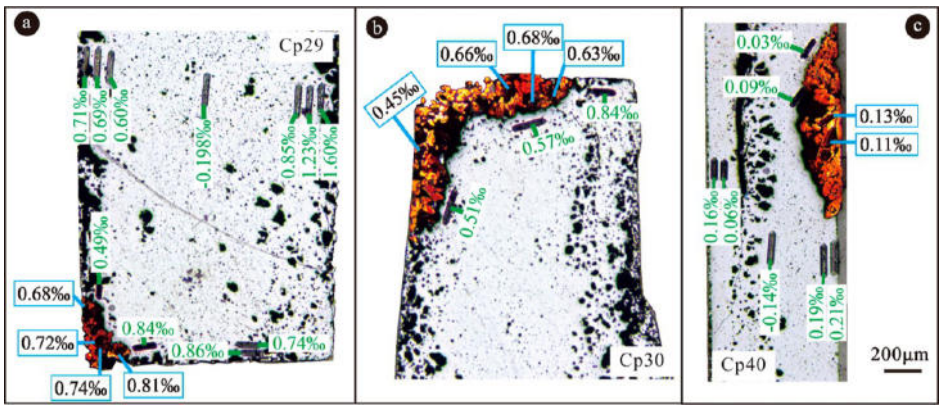

Figure 7. Cu isotope composition of native copper in comparison to cuprite. (a,b) Solids after reaction with 0.2 m HAc/KAc solutions at 250 °C for 24 h. (c) Solids from a temperature cycling run, the temperature was set to 150 °C for 24 h and increased to 250 °C for 24 h and decreased to 150 °C for 24 h and other conditions were fixed. Blue bars refer to analyses of metal and green ones to cuprite analyses.

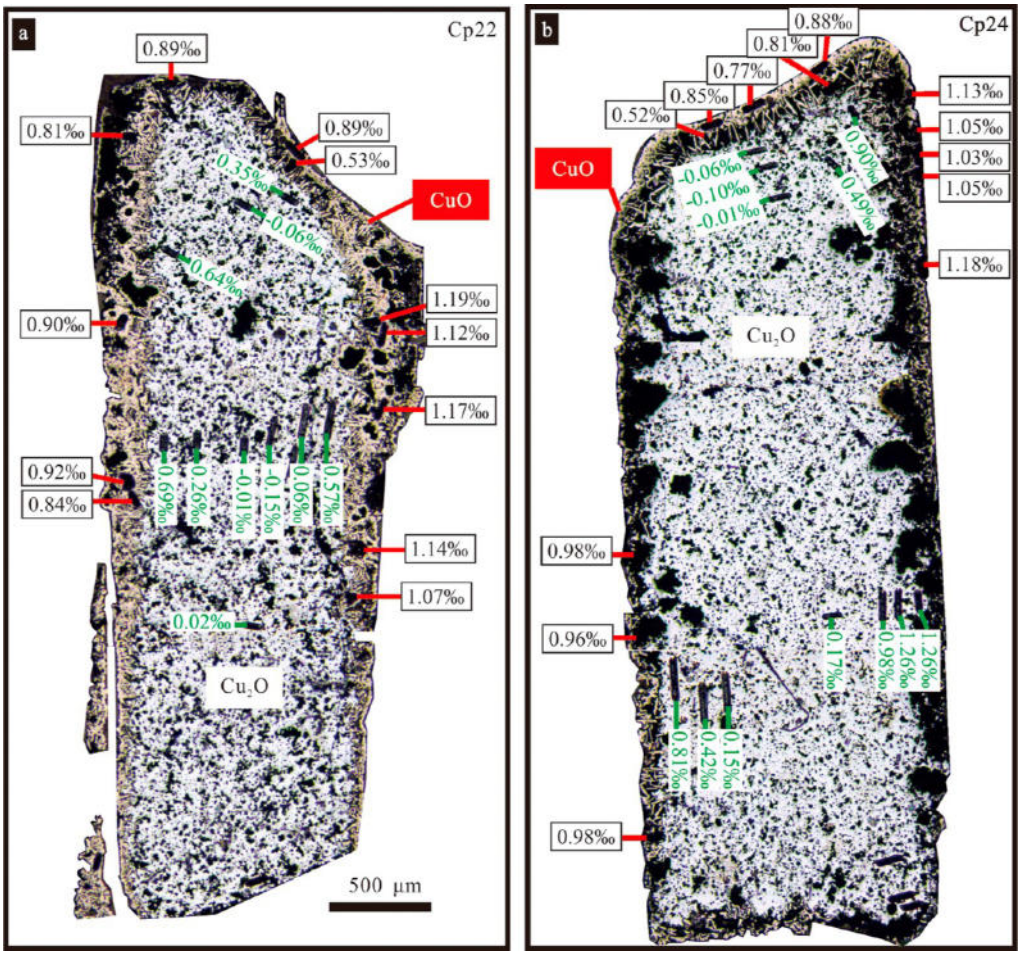

Figure 8. Cu isotope composition of Cu_2O and CuO. Microscopic photos of Cp22 (a) and Cp24 (b) were taken under reflected light. Cp22 and Cp24 were loaded with Cu_2O + 0.2 m HAc/KAc and performed at 150 °C (a) and at 250 °C (b) for 72 h, respectively. Red bars refer to analyses of tenorite.

The contribution by dissolution from the peripheral side is less than 20% and it has been neglected in the first approximation. The estimated uncertainty of the δ^{65}Cu values is 0.08−0.15‰ for the type-II pellets (Table 2).

For type-I pellets, the estimated values of Δx_1 and Δx_2 as well as the corresponding $\delta 1$ and $\delta 2$ values have much higher uncertainty than those for type-II (see Table 2). In general, the effective δ^{65}Cu of dissolved cuprite is higher for type-I than that for type-II, since the isotopically heavy outer layer has been partially removed for type-II samples (Table 2).

4.3.2. Native Copper (Cu). Copper isotope composition was separately determined for metallic Cu deposited on the cuprite pellet (Cu#1) and the gold foil (Cu#2). The overall δ^{65}Cu variation of native Cu is large, e.g., Cu#1 varies from 0.11 ± 0.04 to 0.81 ± 0.04‰ for the samples shown in Figure 7a−c. However, within a single sample, δ^{65}Cu values are fairly constant. For constant temperature runs, Cu#1 shows δ^{65}Cu

https://doi.org/10.1021/acsearthspacechem.3c00254
ACS Earth Space Chem. 2024, 8, 499−519

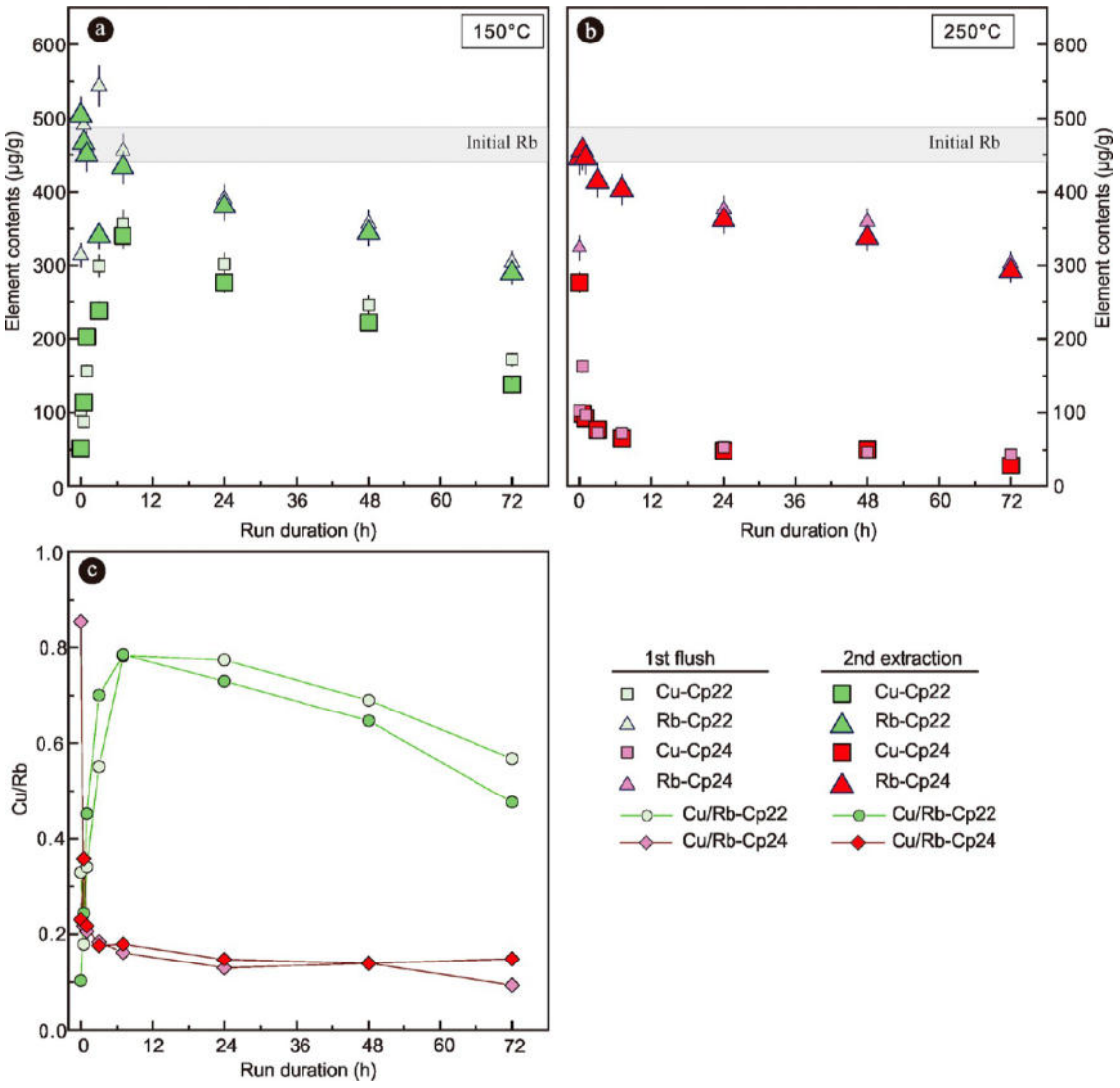

Figure 9. Variation of element contents of solutions as a function of time. (a) Run Cp22, 150 °C, 20 MPa, 72 h; (b) run Cp24, 250 °C, 20 MPa, 72 h. (c) The Cu/Rb ratio (in μg/g) of the 1st and 2nd solutions varies with time. Both experiments were loaded with Cu_2O and 0.2 m HAc/KAc solutions.

values of 0.68 ± 0.04 to 0.81 ± 0.04‰ at 5 MPa, which is up to 0.23 ± 0.06‰ higher than the estimated isotopic composition of the dissolved Cu_2O. At 10 MPa, the δ^{65}Cu value of Cu#1 varies from 0.45 ± 0.03 to 0.68 ± 0.05‰, which is up to 0.21 ± 0.06‰ lower than that of the dissolved Cu_2O. No Cu#2 was found after 6 h, which suggests that its precipitation initiates after 6 h and continues at 24 h. Cu#2 is 0.08 ± 0.05 to 0.39 ± 0.05‰ lower than that of the final solutions from constant temperature runs (Cp29, 30, 31). A temperature cycling experiment was performed at 20 MPa with a time interval of 24 h at 150 and 250 °C. Cu#1 of this run shows little variation in Cu isotope composition, i.e., δ^{65}Cu is 0.12 ± 0.04‰. Cu#1 of Cp40 is up to 0.10 ± 0.06‰ lower than that of the dissolved Cu_2O. The exact timing and temperature of Cu#2 formation are difficult to define. Isotope fractionation between Cu#2 and the final solution at 250 °C is roughly estimated to be −0.60 ± 0.05‰.

4.3.3. Tenorite (CuO). Tenorite formed in long-term runs with 0.2 m HAc/KAc solutions at 150 and 250 °C shows similar large Cu isotopic variation, i.e., from 0.52 ± 0.04 to 1.19 ± 0.04‰ (Figure 8a,b). The lowest values were typically found for the short rims, representing the side planes of the pellets, and the highest values for the long rims, representing the basal planes of the pellet. These trends coincide with the initial copper isotopic distribution in the pellets, as shown in Figure 5. For both experiments, the average δ^{65}Cu of tenorite agrees within error with the δ^{65}Cu values of dissolved cuprite (Table 2). Again, there is a rough correlation between the δ^{65}Cu values of tenorite and those of nearby cuprite. The copper self-diffusion rate in CuO at 250 °C is very low (e.g., $D = 9.3 \times 10^{-26}$ m^2/s, extrapolated from data of Rebane et al.[65]). Once formed, tenorite cannot adjust its Cu isotopic composition to changing conditions by intracrystalline diffusion.

4.4. Temporal Changes in Element Concentrations and pH of the Solution. While solids could only be retrieved after the completion of the experiment, the temporal evolution of the composition of fluids could be monitored in much more detail by intermediate sampling. Well-resolved kinetic trends were obtained for experiments at 150 °C, 20 MPa (Cp22) and 250 °C, 20 MPa (Cp24) over 72 h (Figure 9). With the progressing experiment, the Rb content continuously decreased by ∼30% relative to its initial value (Figure 9a,b). All runs have been performed in single-phase regions of the p, T diagram of H_2O; at 20 MPa up to 200 °C in the liquid field and at 250 °C

https://doi.org/10.1021/acsearthspacechem.3c00254
ACS Earth Space Chem. 2024, 8, 499−519

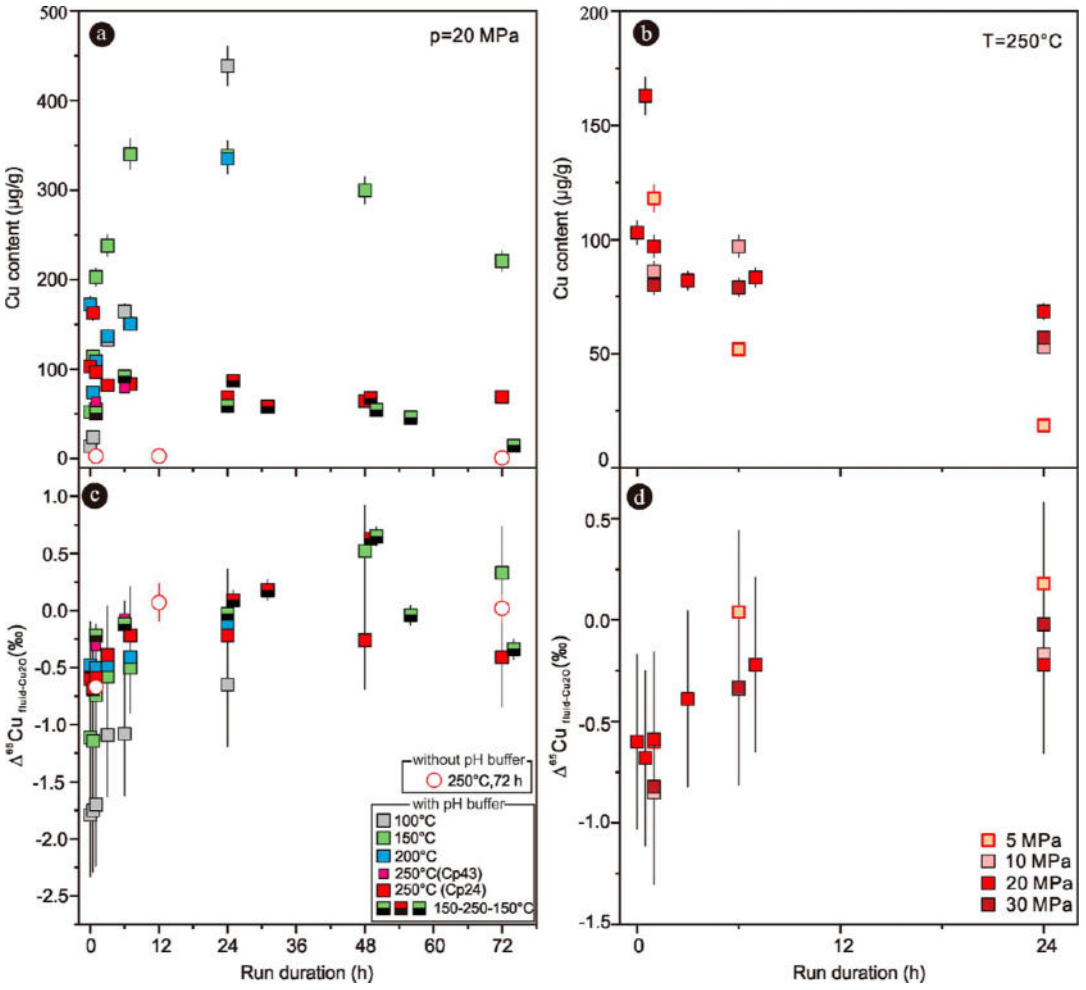

Figure 10. Cu content and copper isotope composition of solutions as a function of run duration. (a,c) Runs were conducted in H_2O or 0.2 m HAc/KAc systems at 20 MPa, 100−250 °C for 6−72 h. (c,d) Runs were performed in 0.2 m HAc/KAc systems at 250 °C, 5−30 MPa for 24 h.

with $p \leq 30$ MPa in the vapor field. Hence, there is no Rb partitioning in the single phase. According to crystal chemistry, the coordination of Cu^{2+} is a distorted octahedron, thus the ionic radius of Cu^{2+} in tenorite should be between 0.73 Å (octahedral coordination) and 0.57 Å (planar square coordination).[66] Rubidium is much larger and has an ionic radius of 1.66 Å in octahedral coordination. Furthermore, cation charges are different for Cu^{2+} and Rb^{+}. Thus, the incorporation of Rb into the newly formed tenorite is very unlikely. The Cu/Rb ratios in fluids are not constant and decrease over time after 24 h in run Cp22 (see Figure 9c). One possible explanation for this is that decarboxylation led to a decrease in both acetate concentration and dissolved Cu content, as discussed below. The decarboxylation of acetate produces gases (detailed in Section 4.6), likely causing Rb to partition into both the fluid and gas phases. The pH of the collected in situ solutions shows only a slight variation over 72 h for the 0.2 m HAc/KAc systems, with pH values ranging from 4.2 to 4.9 (as shown in Table 2). Although the acetate concentration was not measured, the molal ratio of HAc and KAc remains constant. On the other hand, the pH increases from 6.28 to 7.5 after 72 h in the unbuffered H_2O run. Leakage of the Au reaction cell is unlikely to have occurred. First, no Fe was detected in the extracted solutions. Additionally, the fluid inside the Au reaction cell remains transparent after the run, whereas the pressure medium (H_2O) in the steel autoclave turns reddish, suggesting the dissolution of Fe into H_2O. It is worth mentioning that the Ti content in solutions is below the detection limit.

In run Cp22 after 6 h, both the Rb and the Cu concentrations of the second flush are slightly lower than that of the first flush (Figure 9c). In run Cp24, the differences between the first and second solution samples are minor and unsystematic. This difference comes from solution loss during sampling. Except for one sampling (Cp24, 48 h), the δ^{65}Cu values of the first and the second flush agree within 0.2‰ (Table 2). This implies that the small volume of solution in the tubing has only a minor effect on copper isotopes, i.e., there is no significant fractionation in this stagnant solution before sampling. However, this does not apply to the first solution collected when reaching the p, T conditions (t = 0 h). In both experiments, the copper content in the first flush was significantly higher than in the second flush sampled at t = 0 h. A possible explanation is that during p, T equilibration, the volume in the Ti tubing (0.5 mL; cf. chap. 2.2 and Figure 1) may have some memory of previous experiments and, hence, is not representative of the solution in the gold cell. In the latter experiments, the second extracted solution was used for chemical and isotopic analysis, and the first one was used only for pH determination.

4.5. Cu Content in Solution and Its Isotope Fractionation with *t*, *T*, *P*, and pH Buffer. Cu content (C_{Cu}) and Δ^{65}Cu as a function of run time are shown in Figure 10 and tabulated in

https://doi.org/10.1021/acsearthspacechem.3c00254
ACS Earth Space Chem. 2024, 8, 499−519

Table 3. Compositions of Gas Phases in 250 °C and 20 MPa Runs[a]

no.	system	time (h)	CH_4 (nmol)	CO_2 (nmol)	H_2 (nmol)	acetone (nmol)
Cp45	$Cu_2O + H_2O$	72	1	115	<70	0
Cp46	Cu_2O + 0.4 m HAc/KAc	72	31,045	32,351	<70	52

[a]Mineral/fluid ratios of Cp45 and Cp46 are the same as Cp41 and Cp24, respectively.

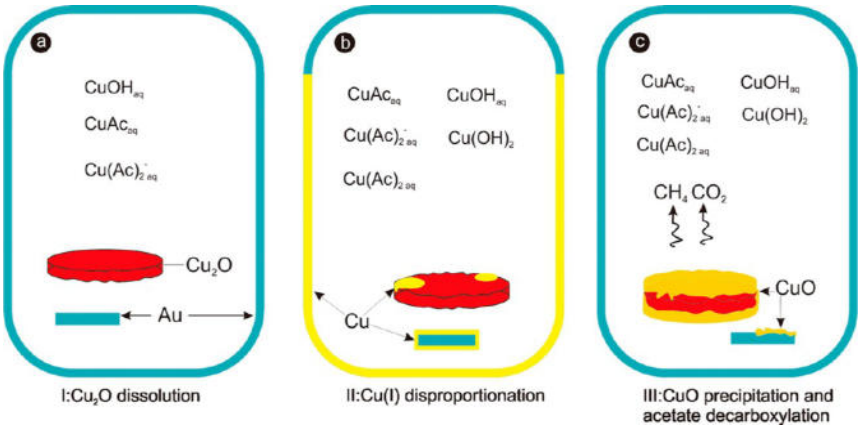

Figure 11. Reaction scheme of cuprite and acetate solution. (a) Cuprite dissolution reaction. (b) Cu(I) disproportionation to Cu(II) and native Cu. (c) Tenorite precipitation and acetate decarboxylation reaction.

Table 2. In the acetate-free system, the C_{Cu} of the solution at 250 °C, 20 MPa decreases from 3.3 to 1.3 μg/g over 72 h.

Much higher copper contents were observed in the acetate bearing system as well as in runs with porous type-I Cu_2O (Figure 10a). Temperature effects are evident for the experimental series at 20 MPa. At 100 °C (Cp27), dissolved Cu increases drastically from 14 to 378 μg/g within 24 h as Cu_2O continuously dissolves from the porous rims. At 150 °C (Cp22), C_{Cu} first increases from 52 to 340 μg/g within 7 h and then decreases to 138 μg/g after 72 h. When reaching stable p, T conditions (t = 0 h) at 200 °C (Cp26), C_{Cu} was relatively high with 173 μg/g. Afterward, C_{Cu} continuously increased from 74 μg/g after 0.5 h to 168 μg/g after 24 h. The long-term experiment at 250 °C (Cp24) yielded a maximum C_{Cu} in the second flush already after 0.5 h with 163 μg/g. Afterward, C_{Cu} continuously decreased to 28 μg/g after 72 h. The short-term experiment at 250 °C (Cp43) yielded a similar C_{Cu} after 6 h (79 μg/g) as Cp24, but for short times, C_{Cu} was much lower in Cp43 (e.g., after 1 h 64 μg/g for Cp43 compared to 97 μg/g for Cp24). The reason could be that a type-II cuprite pellet was used in Cp43. The mechanical removal of the porous outer layer reduced the effective sample surface area, which lowers the dissolution rate. The same effect explains the two-thirds lower Cu contents in the first annealing period at 150 °C for the cycling experiment Cp40 compared to Cp22. A type-II pellet was used in Cp40 as well. In the subsequent period at 250 °C, C_{Cu} of Cp40 was in good agreement with that of Cp24. For the final 24 h period at 150 °C, the Cu content was noticeably lower than in the final stage of the run Cp22, which was held at a constant temperature of 150 °C for 72 h. The comparison of the cycling experiment with the isothermal experiments shows that other parameters besides temperature have a decisive influence on the dissolution behavior of cuprite. A decreasing Cu content correlates with increasing temperature. The possible explanation is that the less dense fluid at high temperatures has a lower ability to dissolve ionic species.

It is worth noting that the mass changes of cuprite are in good agreement with C_{Cu} based on solution analyses for runs without the formation of new phases. Estimated C_{Cu} are 315 μg/g for Cp27 (378 μg/g), 224 μg/g for Cp26 (168 μg/g), and 79 μg/g for Cp43 (79 μg/g). Here, the finally measured C_{Cu} by solution analyses is given in parentheses for comparison. Additionally, residual solutions of Cp27 and Cp43 have 364 and 56 μg Cu/g, respectively, which are comparable to the above values. However, the significant differences between the in situ samples and the quenched solution show how error-prone the analysis of the residual solution can be. In some runs, we observed residual solutions with massive small particles of Cu_2O due to its pellet dissolution, which may lead to higher or lower C_{Cu} than that of the extracted solution.

The experiments for 24 h at 250 °C may give some hints to a possible pressure effect on Cu solubility in acetate-bearing solutions reacted with Cu_2O. The maximum C_{Cu} of the solution increases from 11 μg/g at 5 MPa (Cp29) to 46 μg/g at 10 MPa (Cp30) to 53 μg/g at both 20 (Cp24) and 30 MPa (Cp31). Fluid densities at 5 and 10−30 MPa are 0.80 and 0.81−0.83 g/cm^3, respectively (Driesner and Heinrich (2007)). Fluid at 5 MPa is less dense than those at 10−30 MPa and, hence, ionic species are less well stabilized in solution.

The observed Cu isotope fractionation between extracted fluid and dissolved cuprite, $\Delta^{65}Cu_{fluid-Cu_2O}$, is defined as

$$\Delta^{65}Cu_{fluid-Cu_2O}\,(‰) = \delta^{65}Cu_{fluid} - \delta^{65}Cu_{dissolved\ Cu_2O} \quad (3)$$

A consistent increasing trend of Δ^{65}Cu values with time is found in all runs (Figure 10c,d). All experiments show an increase in the Δ^{65}Cu values of the solution within the first hours (Table 2). After a longer time, the δ^{65}Cu values of the solution are comparable to the average isotopic composition of the dissolved cuprite, i.e., the Δ^{65}Cu values are close to zero. An explanation for this trend could be that cuprite is preferentially dissolved from peripheral planes at the beginning, which has relatively low δ^{65}Cu values (see Figure 5). With increasing time, the basal planes of the pellets, in particular, are dissolved, as can be seen in Figure 6.

https://doi.org/10.1021/acsearthspacechem.3c00254
ACS Earth Space Chem. 2024, 8, 499−519

4.6. Formation of Gases in the Experiments. While the capsule loaded with Cu_2O and H_2O (Cp45) remained flat after the experiment, the capsule containing the acetic acid-acetate–pH buffer (Cp46) expanded, indicating the significant formation of gases. The results of gas phase analyses are tabulated in Table 3. Methane (CH_4) and carbon dioxide (CO_2) are the dominant reaction products in the acetate-bearing system while only trace amounts of these components were measured in the acetate–free system. The similar molar amounts of CH_4 and CO_2 point to a decomposition reaction $CH_3COOH = CO_2 + CH_4$, consistent with findings of Kharaka et al.[18] and Drummond and Palmer[54] and in more complex rock systems with Helten et al.[62] Based on the initial molar amount of acetic acid/acetate of 1.2×10^5 nmol in the gold capsule before the experiment and the measured amount of CH_4 and CO_2, the acetate concentration in the solution was reduced by 25% after 72 h at 250 °C. The pH of solutions of Cp24 (a comparable run of Cp46) was Section 4.6, suggesting that the HAc/Ac ratio was still close to 1. The presence of very small amounts of acetone after run Cp46 points to additional reactions of the decomposition products of acetate, i.e., addition of methyl group units to the acetate ion in solution and forming the C_3-compound acetone. However, due to the low molar amounts of this product, this pathway is not significant for the redox budget in the system. As equimolar amounts of CO_2 and CH_4 have been formed, no CO was detected, and H_2 was below the quantification limit, there is no influence of the decomposition of acetate/acetic acid on the overall redox system in the gold capsule.

5. DISCUSSION

5.1. Reaction Schemes. Based on microscopic observations, phase determinations, element contents (Rb, Cu), and Cu isotope compositions of liquids and solids, three major processes control the reaction of cuprite with acetate-bearing solutions under hydrothermal conditions (Figure 11).

(i) The initial period (up to 24 h at ≤200 °C, up to 6 h at 250 °C) is governed by Cu_2O dissolution. The corresponding reactions in acetate-bearing solutions are

$$Cu_2O_{(s)} + 2HAc_{(aq)} \rightleftharpoons 2Cu(Ac)_{(aq)} + H_2O_{(l)} \quad (4)$$

$$Cu(Ac)_{(aq)} + HAc_{(aq)} \rightleftharpoons Cu(Ac)_2^- + H^+_{(l)} \quad (5)$$

The subscript (aq) is used for neutral species in solution surrounded by H_2O shells; (s) refers to the solid state and (l) to the liquid state. According to Liu et al.,[4] at acetate concentrations as used in our study, the dominant copper species in solution is $CuAc_{(aq)}$ with a minor abundance of $Cu(Ac)_2^-$. Complexes of Cu^+ with OH^- (produced by the disproportion of water, $H_2O = OH^-$ and H^+) are much weaker[52] and not relevant to the conditions of our experiments. The static computation results of Lai et al.[67] suggest that Cu^+ forms linear complexes with one or two acetate ions, rather than with one acetate ion in a nearly symmetric bidentate structure. With increasing acetate concentration and temperature, the proportion of the biacetate complex will become more and more dominating.

The dissolution rate of cuprite is dependent on the available surface area of the solid. This is evident when comparing Cu contents of the solution in the initial stage of experiments Cp22 (using the highly porous type-I cuprite pellet) and Cp40 (using the denser type-II cuprite pellet).

(ii) The second stage involves the formation of native copper via the disproportion reaction

$$2Cu^+_{(aq)} = Cu^{2+}_{(aq)} + Cu_{(s)} \quad (6)$$

Formation of metallic copper by such a reaction was already previously observed, e.g., during leaching of cuprite in oxyacid solution such as sulfuric acid[68−70] or perchloric acid.[71] pH has major control of the Cu(I) disproportionation process, i.e., reaction 6 is favored at pH-values < 6.[72] Using the acetate ionization constant of Mesmer et al.,[53] the pH values of extracted solutions measured at ambient conditions are corrected to be no more than 5.44 at the experimental conditions in our acetate-bearing runs. Similarly, the measured pH of solutions of the $Cu_2O–H_2O$ system corresponds to a value of 4.69 at 250 °C based on the water ionization constant.[73] Thus, in both cases, pH favored the deposition of metallic copper. Another important factor is the nature of the ligand, i.e., acetate stabilizes Cu^{2+} complexes more than Cu^+ complexes, which favors the disproportionation of Cu^+. On the other hand, copper(I) chloride complexes are very stable even at 250 °C, in particular at high chlorine concentrations when $CuCl_2^-$ complexes are formed.[4] Metallic surfaces play a crucial role in the disproportionation reaction. If inert metal surfaces are present such as gold foils, Cu(0) tends to deposit on them.[72] The importance of such metallic surfaces can also be seen in the work of Liu et al.[4] where experiments with acetate solutions in quartz ampules at 150 °C showed no copper deposition even after 9 days. As can be seen in Figure 7, copper deposition on cuprite is localized and penetrates into the pellet while the overall shape of the pellet has been maintained. This indicates a replacement reaction, i.e., Cu^+ formed during the dissolution of cuprite is redeposited directly next to it on the metal surface via the disproportionation reaction. The uneven coverage of the cuprite surface with metal precipitates points to the high nucleation energy for metallic copper in hydrothermal solutions. This effect may contribute to the formation of massive native copper deposits in some areas such as the Keweenaw mines in Michigan.[74] Native silver may act as a metallic surface resulting in the formation of metallic copper; the aqueous Cu^{2+} in solution would nucleate into iron oxyhydroxides and finally lead to the formation of hematite in the Keweenaw mines.[72,75]

(iii) The third stage is an oxidation reaction associated with the redissolution of metallic copper and the formation of tenorite. Native copper survived in the 72 h experiment in the acetate-free experiment Cp41 at 250 °C, and no tenorite was formed, giving evidence that the oxidation reaction in the solution is due to acetate or acetic acid. On the one hand, masses of Cu from Cp29, 30, 31 are estimated to be about 0.08–0.15 g (e.g., Figure 2c), and it needs 70–132 mL of air (approximately 14–26 mL O_2) to oxidize Cu to CuO at 25 °C, 0.1 MPa. This is inconsistent with the fact that the solution was fully filled before the run. On the other hand, Kharaka et al.[18] systematically studied the stability of acetate-containing solutions under hydrothermal conditions in a stainless-steel autoclave. They found that acetate is very stable in solutions even at 300 °C, while acetic acid decomposes into methane and carbon dioxide in a first-order reaction. The half-life time $t_{1/2}$ at 250 °C derived from our run Cp46 is only 3 days, while from the data of Kharaka et al.,[18] a much longer $t_{1/2}$ of 195 days would be expected. As demonstrated by Palmer and Drummond,[19] gold surfaces

https://doi.org/10.1021/acsearthspacechem.3c00254
ACS Earth Space Chem. 2024, 8, 499–519

have no promoting effect on the decomposition of acetic acid. Moreover, they found that dissolved transition metal ions (Fe^{2+} and Cr^{3+}) did not act as homogeneous catalysts in the solution. However, findings of[62] point to the possible influence of minerals in the reactions for the decomposition reaction.

Hence, we conclude that cuprite is actively involved in the reaction. A strong catalytic effect of cuprite can be inferred also from the experiments of Liu et al.[4] The explosion of silica ampules after experiments with cuprite and acetic solutions at 250 °C indicates intensive production of gas components (i.e., CH_4 and CO_2). A catalytic effect of the silica glass surface can be excluded after the experiments of Palmer and Drummond.[19] On the other hand, Palmer and Drummond[19] noted that magnetite strongly speeds up the reaction by heterogeneous catalysis. They found that at 350 °C, more than 25% of the initial acetic acid had reacted within the first 70 h. Our findings as well as those of[4] suggest that cuprite may have an even much stronger catalytic effect on the decomposition of acetic acid, i.e., electron transfer with transition metals plays an important role. However, it is out of the scope of our study to analyze the kinetics of the reaction in detail.

The mechanism of the oxidation reaction is still rather unclear and probably very complex. The decomposition of acetic acid produces approximately equal proportions of methane and carbon dioxide. Oxidation of copper species is not associated with this reaction. The increase of Cu^+ in the solution can lead to supersaturation and redeposition of cuprite (reactions 4 and 5). Alternatively, it can be directly oxidized into Cu^{2+}, which then causes supersaturation of the solution with tenorite. Based on our experiments, we cannot decide which of these processes takes place because solid samples after intermediate times are missing. From a thermodynamic point of view, it is very unlikely that three phases with three different oxidation states of copper coexist. However, one must be aware that it is a disequilibrium system and cannot exclude such a situation. In any case, the shape of the postexperimental pellets with the uniform tenorite layer is a clear indication that the dissolved metal zones in the pellets were redeposited on-site by a dissolution−precipitation process. The replacement of native Cu and Cu_2O by CuO had been confirmed by Raman analysis (Figure 4); however, this oxidation process remains unclear. These tenorite crystals are found to deposit on the Au foil and formed directly adjacent to the dissolved cuprite possibly via

$$Cu(Ac)_{2(aq)} + H_2O_{(l)} = CuO_{(s)} + 2HAc_{(aq)} \quad (7)$$

The precipitation of the tenorite on Au foil suggests a reaction mechanism involving the direct deposition of the tenorite from the solution.

The structure of the tenorite layer around the cuprite pellet (Figure 8) is very similar to the congruent crystallization of glass plates (e.g., plagioclase glasses[76]). In the beginning, tenorite crystals randomly deposit all around the pellet. These crystals are rather small and have random orientations. With progressing reaction, the crystals with preferred orientation are favored and grow to a larger size. This topology supports scenarios including local dissolution−precipitation reactions.

In any case, the driving force of tenorite formation is the high concentration of Cu^{2+} in the solution. Formation of metal oxide from acetate solution can also be found elsewhere (e.g., TiO_2).[19] They found that a high concentration of titanium acetate ($Ti(Ac)_{2+n}^{n-}$) in the solution can lead to a significant amount of recrystallization of TiO_2.

Replacement of cuprite by native Cu and by tenorite indicates that dissolution and precipitation of these phases proceed from the surface to the interior of Cu_2O (Figures 2c−f, 7 and 8). This in situ precipitation is in accord with the observation in oxidation zones, where Cu did not take a long path, but most of the cuprite and native Cu were directly precipitated almost in situ.[17] This process is similar to the pseudomorphic copper sulfide replacement reactions.[77,78] These textures are controlled by a CDR mechanism. CDR is the predominant process, especially in the presence of fluids at a temperature lower than 300 °C, and it occurs rather fast (4−360 h) in the study of Adegoke et al.[77] The precipitation of Cu and tenorite on Cu_2O as well as on the Au foil demonstrates that nucleation and growth rates are high for tenorite in these systems. It should be emphasized that Cu diffusion in cuprite and tenorite is too slow at the experimental conditions to explain the replacement by solid-state diffusion. Large pores found in the tenorite layer serve as a pathway for mass transport between the surrounding local fluid and the reaction front.

5.2. Cu Contents of Solutions and Cuprite Solubility. It is striking that the Cu contents of the solutions determined in the initial period of the experiments are drastically higher than the Cu solubilities reported by Liu et al.[4] For instance, according to Liu et al.,[4] the copper solubility in a 0.2 m NaAc/HAc solution at 150 °C is 9 μg/g, while the copper content of a 0.2 m KAc/HAc solution in run Cp22 was already 340 μg/g (2nd flush, see Table 2) after 7 h. Taking minor RbCl (0.004 m) into consideration, our data are higher by a factor of 8 than that of Liu et al.,[4] i.e., 340 and 44 μg/g Cu, respectively. The differences are likely due to the experimental and analytical procedures in the two studies. Liu et al.[4] applied the silica tube technique which is well-established from previous studies.[79] After cooling, they used a syringe equipped with a microfilter (0.45 μm) to withdraw the solution from the area of the silica ampule separated by a narrow constriction from the area containing a cuprite pellet. Constant copper contents of the solution were reached within 2 weeks at 50 °C and within 48 h at 150 °C for sodium acetate solutions, which was taken as evidence for the attainment of equilibrium.

In our experiments, the variation in the copper content of the solutions suggests that chemical equilibrium was not attained, which is likely due to the progressive acetate decomposition after a certain time. Thus, only minimum values for cuprite solubility in acetate-bearing solutions can be derived from our experiments. At 100 °C, the copper content of 378 μg/g (Cp27, second flush) in the solution was determined at a time when the acetate concentration had decreased by 14% based on the Rb data. Acetate decomposition is not expected at this low temperature. At 150 °C (Cp22), the maximum Cu content of 340 μg/g (2nd flush) after 7 h is probably close to the equilibrium value for the 0.2 m KAc/HAc solution. The constant Rb contents suggest a minor effect of acetate decomposition and little Rb partitioning into vapor ($CO_{2(g)}$, $CH_{4(g)}$) at this time. The strong decrease of Cu content between 24 and 72 h is attributed to the oxidation to tenorite, induced by the decomposition of acetate. At 200 °C (Cp26), the copper content continuously increased up to 168 μg/g after 24 h, although the Rb content was already lowered by 50% at that time. Acetate concentration is reduced at least to the same extent, which should lead to a decrease in cuprite solubility. This implies that the measured C_{Cu} after 24 h is still well below the

https://doi.org/10.1021/acsearthspacechem.3c00254
ACS Earth Space Chem. 2024, 8, 499−519

cuprite solubility. At 250 °C, the initial dissolution of cuprite is followed by disproportion and oxidation reactions, and a clear statement on cuprite solubility is not possible.

The large difference from the previous study cannot be explained by the different pressures in the experiments (vapor pressure of 5 MPa in Liu et al.,[4] and hydrostatic pressure of 20 MPa in our experiment), since our experiments at 250 °C do not indicate a significant pressure effect in the range of 5−30 MPa. Furthermore, solubility data for cuprite in 0.5 m chlorine-bearing solutions reported by Liu et al.[4] are in good agreement with the experiments of Qi,[80] applying the same approach as presented here. Thus, it is unlikely that the high Cu contents of the acetate solutions in our study are due to the insufficient retention of solid microparticles by the titanium filter used in the experiments. A possible explanation for the discrepancy is that when the acetate solution cools to room temperature, solids are precipitated and then retained by the filter attached to the syringe in the study by Liu et al.[4] In that case, the copper solubility would be underestimated by analysis of the received solution. This problem is avoided when filtering and liquid extraction are done at the experimental temperature. However, further tests are required to support this hypothesis.

Although our experiments have not yielded definitive solubility data, they do show that acetate is almost as effective as a complexing agent for copper in solutions as chlorine. At a comparable HAc-KAc concentration to this study, Liu et al.[4] report that cuprite solubility in NaCl solution positively correlates to temperature, e.g., C_{Cu} in 0.1 M NaCl increases from 437 to 601 and 669 ppm at 50, 150, and 250 °C, respectively. The Cl-bearing solution dissolves more Cu_2O than the Ac-bearing solution, e.g., at pH of 4.6 dissolved Cu in NaCl solution are 2 and 20 times higher than that in Ac solution according to our study and Liu et al.,[4] respectively. Although our data for Ac-bearing solutions are higher than those determined by Liu et al.,[4] the solubility trend is consistent with the increasing strength of the ligand from OH^- to Ac^- and Cl^-.

5.3. Cu Isotope Fractionation and the Controlling Mechanism for the Cu_2O-HAc-KAc Alteration Process. At the initial stage of the reaction, no new minerals are formed, and hence cuprite dissolution is only a one-way reaction. Furthermore, diffusion of copper in cuprite is too slow, to readjust the copper isotopic composition inside the cuprite with dissolved copper species in the solution. Thus, the copper isotopic composition of the solution equals to that of the dissolved cuprite.

Several processes are involved in the second stage of the reaction, i.e., cuprite dissolution, native copper precipitation, and partial oxidation of Cu^+ to Cu^{2+} in the solution. It is worth mentioning that native Cu formed in a single run but at different localities yields different δ^{65}Cu values, e.g., from 0.61 ± 0.09 to 1.13 ± 0.04‰ in Cp30 (Table 2). Large isotope composition variation during precipitation of native Cu has been reported elsewhere, e.g., Dekov et al.[81] observed Cu isotope variations between 0.41 and 0.95‰ for native copper from sedimentary layers. Likely, these Cu isotope compositions indicate a different mechanism of Cu precipitation. The copper metal deposited on cuprite by the CDR process displays isotope signatures similar to their adjacent cuprite (Figure 7), i.e., $\Delta^{65}Cu_{Cu\#1-Cu_2O}$ values are −0.32 ± 0.06‰ for Cp29, −0.15 ± 0.06‰ for Cp30, and −0.10 ± 0.06‰ for Cp40. Isotopic data of Cu precipitated on the Au surface (Cu#2) far away from the source cuprite are difficult to interpret, since the timing of its formation is hardly defined. A rough estimation can be made based on the difference in δ^{65}Cu between the last collected solution and the copper layer on the gold foil, i.e., $\Delta^{65}Cu_{Cu\#2-fluid}$ values are −0.31 ± 0.05‰ for Cp29, −0.08 ± 0.05‰ for Cp30, −0.39 ± 0.05‰ for Cp31, and −0.62 ± 0.05‰ for Cp40. These negative values might indicate that Cu does not precipitate from the final solution, and the precipitation might occur early. The final collected solutions display a similar copper isotope composition as the average value for the dissolved cuprite, i.e., $\Delta^{65}Cu_{fl-Cu_2O}$ values of 0.02 ± 0.08 and −0.06 ± 0.43‰ in Cu_2O−H_2O and Cu_2O-HAc-KAc systems, respectively. In all cases, the isotopic data at this stage of the reaction reflected kinetic fractionation as the involved phases either dissolved or formed and no equilibrium could be reached due to slow intracrystalline diffusion. Cuprite had only dissolved, but not reprecipitated, and the metal had not redissolved during this stage.

Different reactions compete at the third stage, e.g., the Cu metal is redissolved, the dissolution of the cuprite proceeds, and a new phase (tenorite) is formed. Conclusions about Cu isotope fractionations during Cu metal dissolution are not possible, since solid run products including both native copper and tenorite were not retrieved. Tenorite crystals on the cuprite pellet have variable isotope signatures due to the initial copper isotope variations of the pellet and as a result their formation at different stages. However, tenorite and adjacent cuprite have very similar δ^{65}Cu. This finding supports the hypothesis that tenorite likely formed during a CDR process, i.e. a near-site deposition of the dissolved copper, which is not expected to result in significant Cu isotope fractionation.

5.4. Implications. Cu metal transport by acetic acid/acetate may play a vital role in (1) the formation of sediment-hosted stratiform Cu ore[82] and (2) Cu precipitation during its reaction with sulfate.[83] Sediment-hosted stratiform Cu ores account for a significant portion of the world's Cu production, e.g., ca. 180 Mt at Copperbelt in Zambia[84] and ca. 3.3 Mt at White Pine native Cu mine in the United States.[85] Up to 0.08 m (i.e., 4900 μg/g) of aliphatic acid (possibly acetic acid) has been detected in sedimentary basin brines at San Emidio Nose oil field, California.[9] Previous studies have stated that the ppm level of Cu (typically 5−50 μg/g) in the solution is enough to form such a tonnage of Cu ores.[85,86] Our data imply that hundreds of ppm of Cu may have been transported by acetate-bearing fluids and subsequent metal precipitation due to the instability of the complexing ligand may explain the enrichment of copper in sediment-hosted Cu ore deposits.

Copper isotope fractionation related to the redox process within fluids or between fluid and solid are well-known, i.e., Δ^{65}Cu values up to 4‰ were observed in both experiments and in natural samples.[25,27,29,32,33,35] In contrast, little is known about the fractionation of copper isotopes during mineral replacement reactions, which proceed from a parent mineral dissolution to the daughter mineral precipitation.[77,87] Such reactions often involve changes in the oxidation state of metals, e.g., during the replacement of chalcopyrite by covellite and digenite.[78] Copper isotope fractionation can be associated with such reactions if the initial Cu mineral is replaced by Cu species with different oxidation states and subsequently, these species are physically separated from each other. For example, Rouxel et al.[26] analyzed secondary Cu(II)-bearing phases such as atacamite, digenite, and covellite, which encrusted the primary chalcopyrite during low-temperature sea-floor hydrothermal alteration. They state that secondary copper phases yield 3‰

https://doi.org/10.1021/acsearthspacechem.3c00254
ACS Earth Space Chem. 2024, 8, 499−519

heavier copper isotopic values than the primary Cu(I) mineral. Asael et al.[30,31] report that Cu(II) minerals (malachite, paratacamite, and tenorite), which replaced Cu−sulfide, are up to 3.86‰ heavier than the parent (djurleite, chalcocite, and covellite) in sedimentary hosted Cu deposits.

A recent study by Chaudhari et al.[78] shows that the Cu isotope composition can be reset during the replacement and recrystallization reactions of chalcopyrite in the presence of a ^{65}Cu-enriched aqueous fluid. However, the experiments were conducted under extreme conditions, i.e., the copper content and the amount of solution were already very high at the beginning of the experiment. This resulted in the preferential replacement of ^{63}Cu in the parent chalcopyrite by ^{65}Cu in the daughter mineral. In our experiments, the replacement of cuprite by metallic Cu and subsequently by tenorite in HAc/KAc solution at 250 °C and 20 MPa did not induce significant isotope fractionation, although changes in the oxidation state of copper are involved. These findings are consistent with observations of Markl et al.[88] who report fractionations of only 0.16−0.5‰ during the oxidation of Cu_2O to malachite in the Scharzwald mining district. On the other hand, our trends are quite different from the data of Rouxel et al.[26] and Asael et al.[30,31] In comparison to insignificant isotope fractionation in this study, they[26,30,31] observe isotope fractionation up to 3‰ due to stronger complexing ligands (S and/or Cl) and lower temperatures than those of this study.

In geological settings, the formation of native copper from a Cu(I) or Cu(II) source is attributed to an abiotic (methane) or biotic (organic compounds) reduction process.[81,88] Our study shows that cuprite itself can act as a reducing agent, and the disproportionation of dissolved Cu^+ can lead to the formation of copper deposits under certain conditions. Moreover, it may offer an alternative explanation for the co-occurrence of cuprite and native Cu in the supergene environment.[89] Interestingly, this and other studies show that the reduction-related isotope fractionation is minor.[35,88]

A technological aspect of our studies concerns the formation of tenorite layers on substrates. CuO is of great interest due to its potential application in the semiconductor material, solar cells, gas sensors, and catalysts.[90] Previous studies show that CuO can be synthesized from $Cu(Ac)_2$ through various techniques, such as the solvothermal method,[91,92] precipitation method,[93] atmospheric decomposition,[94,95] and sol−gel-like processing.[96] In our experiments, submicroscopic tenorite layers were deposited on substrates from solutions via a continuous oxidation process initiated by the decomposition of acetate. Observations on both the metal foils and the cuprite pellets indicate that nucleation energy for tenorite is low in aqueous acetate solutions. Furthermore, it shows an interesting possibility to fabricate sandwich interconnects of two different semiconductors (Cu_2O and CuO).

6. CONCLUSIONS

The reaction of cuprite (Cu_2O) with pH-buffered (0.2 m HAc/KAc) hydrothermal fluids was experimentally investigated at temperatures of 100−250 °C and pressures of 5−30 MPa. A cuprite pellet, a piece of Au foil, and the solution were loaded in a flexible gold reaction cell inside a steel autoclave held at constant pressure. In situ fluid sampling enabled the determination of quenched pH, dissolved copper contents, and isotopic compositions of the fluid at different stages of the reaction. The copper isotopic composition of solid phases was analyzed using LA-MC-ICP-MS. Relict cuprite was observed in all runs. Massive native copper partially or fully covering the Au cell as well as foil and locally replacing cuprite have been detected in acetate-bearing and acetate-free systems after 24 h at 250 °C. When the run duration was extended to 72 h, tenorite (CuO) replaced native copper and fully covered cuprite and was deposited on the Au foil as well at both 150 and 250 °C. These observations can be explained by a three-step process: (i) dissolution kinetics of cuprite occurs at 100−200 °C for 24 h and 250 °C for 6 h, with Cu^+ as the predominant species in the solution. (ii) Disproportionation of dissolved Cu^+ into Cu metal and dissolved Cu^{2+} occurs at high temperature (250 °C) between 6 and 24 h, which is driven by the high bonding energy in Cu(II) acetate complexes. (iii) Decomposition of acetate occurs at 250 °C, >24 h and 150 °C, 72 h. Concomitantly, this accompanies the oxidation of Cu^0 and Cu^+ to Cu^{2+} and a decrease in complexing agent concentration. This reaction triggers the formation of tenorite.

Full equilibrium between cuprite and solution was not achieved at a low temperature of 100−200 °C and minimum values of cuprite solubility were estimated from the time evolution of Cu contents of the solutions for 100−200 °C, i.e., 378 μg Cu/g at 100 °C, 340 μg/g at 150 °C, and 168 μg/g at 200 °C. At 250 °C, cuprite solubility cannot be estimated due to different reactions competing in the system. Linear regression yields $C_{Cu} = 3.3 \pm 0.2 + (-0.05 \pm 0.001) \times T$, where T is in Celsius. Interpretation of the copper isotopic data is complicated since the cuprite pellets already contained isotopic gradients imposed by sintering. In the first and second stages, the copper isotope composition of the solution was similar to the mean value of the dissolved cuprite. No significant influence of the pressure was found at 250 °C neither for the Cu contents nor for the copper isotope composition of the fluid in the range of 5−30 MPa. The in situ measured δ^{65}Cu value for native copper is similar to that of adjacent cuprite, mostly clustering at 0.15 ± 0.06‰. Including native Cu precipitation on the Au substrate the overall $\Delta^{65}Cu_{Cu-Cu(I)}$ is within 0.32 ± 0.06‰. Likewise, the δ^{65}Cu of the tenorite is close to that of the adjacent cuprite. These findings suggest that the replacement reactions are controlled by a CDR mechanism, i.e., the released dissolved copper is directly and quantitatively incorporated into the newly formed solid phases.

The Cu content in the Ac-bearing solution in this study is much higher than that reported in the literature.[4] The temperature is inversly related to dissoved Cu in acetate system, and hence this indicates that the potential of acetate-bearing solutions to transport copper may be much higher than expected at low temperatures. Furthermore, the transport of hundreds of ppm of Cu by acetate-bearing solutions is a strong indication that acetate is an effective complexing agent for copper in hydrothermal fluids, especially in sedimentary settings.

AUTHOR INFORMATION

Corresponding Author

Dongmei Qi − *Institute of Mineralogy, Leibniz University of Hannover, 30167 Hannover, Germany; Xinjiang Key Laboratory for Geodynamic Processes and Metallogenic Prognosis of the Central Asian Orogenic Belt, Department of Geology and Mining Engineering, Xinjiang University, 830046 Urumqi, China;* orcid.org/0000-0002-5238-7038; Email: dongmei.qi@xju.edu.cn

https://doi.org/10.1021/acsearthspacechem.3c00254
ACS Earth Space Chem. 2024, 8, 499−519

Authors

Harald Behrens − *Institute of Mineralogy, Leibniz University of Hannover, 30167 Hannover, Germany*

Marina Lazarov − *Institute of Mineralogy, Leibniz University of Hannover, 30167 Hannover, Germany*

Roman Botcharnikov − *Institute of Geosciences, Johannes Gutenberg University Mainz, 55128 Mainz, Germany*

Chao Zhang − *State Key Laboratory of Continental Dynamics, Department of Geology, Northwest University, 710069 Xi'an, China*

Christian Ostertag-Henning − *Federal Institute for Geosciences and Natural Resources (BGR), 30655 Hannover, Germany*

Stefan Weyer − *Institute of Mineralogy, Leibniz University of Hannover, 30167 Hannover, Germany;* orcid.org/0000-0001-7734-4571

Complete contact information is available at: https://pubs.acs.org/10.1021/acsearthspacechem.3c00254

Notes

The authors declare no competing financial interest.

■ ACKNOWLEDGMENTS

This research was supported by the National Natural Science Foundation of China (41972055, 42002059), Open Project of Key Laboratory, Xinjiang Uygur Autonomous Region, China (2023D04067), the Key Research and Development Program of Xinjiang Uygur Autonomous Region, China (2022B03015-2), and the German Academic Exchange Service (DAAD-57076462). We thank U. Kroll, A. Reimer, and J. Feige for their technical support and D. Graskamp and J. Poggenburg for the gas chromatographic analyses. We are grateful to three anonymous reviewers, and the Associate Editor Sumit Chakraborty for their constructive comments and revisions that greatly improved the quality of the manuscript.

■ REFERENCES

(1) Leach, D. L.; Bradley, D. C.; Huston, D.; Pisarevsky, S. A.; Taylor, R. D.; Gardoll, S. J. Sediment-Hosted Lead-Zinc Deposits in Earth History. *Econ. Geol.* **2010**, *105* (3), 593−625.

(2) Sverjensky, D. A. The role of migrating oil field brines in the formation of sediment-hosted Cu-rich deposits. *Econ. Geol.* **1987**, *82* (5), 1130−1141.

(3) Xiao, Z.; Gammons, C. H.; Williams-Jones, A. E. Experimental study of copper(I) chloride complexing in hydrothermal solutions at 40 to 300°C and saturated water vapor pressure. *Geochim. Cosmochim. Acta* **1998**, *62*, 2949−2964.

(4) Liu, W.; McPhail, D. C.; Brugger, J. An experimental study of copper(I)-chloride and copper(I)-acetate complexing in hydrothermal solutions between 50 °C and 250 °C and vapor-saturated pressure. *Geochim. Cosmochim. Acta* **2001**, *65* (17), 2937−2948.

(5) Disnar, J. R.; Sureau, J. Organic matter in ore genesis: Progress and perspectives. *Org. Geochem.* **1990**, *16*, 577−599.

(6) Kucha, H. Precious metal alloys and organic matter in the Zechstein copper deposits, Poland. *TMPM, Tschermaks Mineral. Petrogr. Mitt.* **1981**, *28* (1), 1−16.

(7) Giordano, T. H. A preliminary evaluation of organic ligands and metal-organic complexing in mississippi valley-type ore solutions. *Econ. Geol.* **1985**, *80* (1), 96−106.

(8) Willey, L. M.; Kharaka, Y. K.; Presser, T. S.; Rapp, J. B.; Barnes, I. Short chain aliphatic acid anions in oil field waters and their contribution to the measured alkalinity. *Geochim. Cosmochim. Acta* **1975**, *39* (12), 1707−1711.

(9) Carothers, W. W.; Kharaka, Y. K. Aliphatic acid anions in oil-field waters-implications for origin of natural gas. *AAPG Bull.* **1978**, *62* (12), 2441−2453.

(10) Cordell, R. J. Depths of oil origin and primary migration: a review and critique. *AAPG Bull.* **1972**, *56* (10), 2029−2067.

(11) Meyers, P. A.; Pratt, L. M.; Nagy, B. Introduction to geochemistry of metalliferous black shales.**1992**.

(12) Ruffell, A. H.; Moles, N. R.; Parnell, J. Characterisation and prediction of sediment-hosted ore deposits using sequence stratigraphy. *Ore Geol. Rev.* **1998**, *12* (4), 207−223.

(13) Coveney, R. M. Metalliferous Paleozoic black shales and associated strata. *Geol. Sediment. & Sedimentary Rocks* **2003**, *4*, 135−144.

(14) Dold, B.; Blowes, D. W.; Dickhout, R.; Spangenberg, J. E.; Pfeifer, H. R. Low Molecular Weight Carboxylic Acids in Oxidizing Porphyry Copper Tailings. *Environ. Sci. Technol.* **2005**, *39* (8), 2515−2521.

(15) Vasconcelos, P. M.; Reich, M.; Shuster, D. L. The paleoclimatic signatures of supergene metal deposits. *Elements* **2015**, *11* (5), 317−322.

(16) Williams, W. C.; Meissl, E.; Madrid, J.; De Machuca, B. C. The San Jorge porphyry copper deposit, Mendoza, Argentina: a combination of orthomagnatic and hydrothermal mineralization. *Ore Geol. Rev.* **1999**, *14* (3−4), 185−201.

(17) Chávez, W. X. Supergene Oxidation of Copper Deposits: Zoning and Distribution of Copper Oxide Minerals. *SEG Discovery* **2000**, *41*, 1−21.

(18) Kharaka, Y. K.; Carothers, W. W.; Rosenbauer, R. J. Thermal decarboxylation of acetic acid: implications for origin of natural gas. *Geochim. Cosmochim. Acta* **1983**, *47* (3), 397−402.

(19) Palmer, D. A.; Drummond, S. E. Thermal decarboxylation of acetate. Part I. The kinetics and mechanism of reaction in aqueous solution. *Geochim. Cosmochim. Acta* **1986**, *50* (5), 813−823.

(20) Mathur, R.; Titley, S.; Barra, F.; Brantley, S.; Wilson, M.; Phillips, A.; Munizaga, F.; Maksaev, V.; Vervoort, J.; Hart, G. Exploration potential of Cu isotope fractionation in porphyry copper deposits. *J. Geochem. Explor.* **2009**, *102* (1), 1−6.

(21) Lv, Y.; Liu, S. A.; Zhu, J. M.; Li, S. Copper and zinc isotope fractionation during deposition and weathering of highly metalliferous black shales in central China. *Chem. Geol.* **2016**, *445*, 24−35.

(22) Rempel, K. U.; Liebscher, A.; Meixner, A.; Romer, R. L.; Heinrich, W. An experimental study of the elemental and isotopic fractionation of copper between aqueous vapour and liquid to 450°C and 400bar in the CuCl−NaCl−H2O and CuCl−NaHS−NaCl−H2O systems. *Geochim. Cosmochim. Acta* **2012**, *94*, 199−216.

(23) Guo, H.; Xia, Y.; Bai, R.; Zhang, X.; Huang, F. Experiments on Cu-isotope fractionation between chlorine-bearing fluid and silicate magma: Implications for fluid exsolution and porphyry Cu deposits. *Natl. Sci. Rev.* **2020**, *7* (8), 1319−1330.

(24) Plumhoff, A. M.; Mathur, R.; Milovský, R.; Majzlan, J. Fractionation of the copper, oxygen and hydrogen isotopes between malachite and aqueous phase. *Geochim. Cosmochim. Acta* **2021**, *300*, 246−257.

(25) Ehrlich, S.; Butler, I.; Halicz, L.; Rickard, D.; Oldroyd, A.; Matthews, A. Experimental study of the copper isotope fractionation between aqueous Cu(II) and covellite, CuS. *Chem. Geol.* **2004**, *209* (3−4), 259−269.

(26) Rouxel, O.; Fouquet, Y.; Ludden, J. N. Copper isotope systematics of the Lucky Strike, Rainbow, and Logatchev sea-floor hydrothermal fields on the Mid-Atlantic Ridge. *Econ. Geol.* **2004**, *99* (3), 585−600.

(27) Mathur, R.; Ruiz, J.; Titley, S.; Liermann, L.; Buss, H.; Brantley, S. Cu isotopic fractionation in the supergene environment with and without bacteria. *Geochim. Cosmochim. Acta* **2005**, *69* (22), 5233−5246.

(28) Haest, M.; Muchez, P.; Petit, J. C.; Vanhaecke, F. Cu isotope ratio variations in the Dikulushi Cu-Ag deposit, DRC: of primary origin or induced by supergene reworking? *Econ. Geol.* **2009**, *104* (7), 1055−1064.

(29) Kimball, B. E.; Mathur, R.; Dohnalkova, A. C.; Wall, A. J.; Runkel, R. L.; Brantley, S. L. Copper isotope fractionation in acid mine drainage. *Geochim. Cosmochim. Acta* **2009**, *73* (5), 1247−1263.
(30) Asael, D.; Matthews, A.; Oszczepalski, S.; Bar-Matthews, M.; Halicz, L. Fluid speciation controls of low temperature copper isotope fractionation applied to the Kupferschiefer and Timna ore deposits. *Chem. Geol.* **2009**, *262* (3−4), 147−158.
(31) Asael, D.; Matthews, A.; Bar-Matthews, M.; Harlavan, Y.; Segal, I. Tracking redox controls and sources of sedimentary mineralization using copper and lead isotopes. *Chem. Geol.* **2012**, *310*−*311*, 23−35.
(32) Fernandez, A.; Borrok, D. M. Fractionation of Cu, Fe, and Zn isotopes during the oxidative weathering of sulfide-rich rocks. *Chem. Geol.* **2009**, *264* (1−4), 1−12.
(33) Zhu, X. K.; Guo, Y.; Williams, R. J. P.; O'Nions, R.; Matthews, A.; Belshaw, N.; Canters, G.; de Waal, E.; Weser, U.; Burgess, B.; et al. Mass fractionation processes of transition metal isotopes. *Earth Planet. Sci. Lett.* **2002**, *200* (1−2), 47−62.
(34) Pękala, M.; Asael, D.; Butler, I. B.; Matthews, A.; Rickard, D. Experimental study of Cu isotope fractionation during the reaction of aqueous Cu(II) with Fe(II) sulphides at temperatures between 40 and 200°C. *Chem. Geol.* **2011**, *289* (1−2), 31−38.
(35) Qi, D.; Behrens, H.; Lazarov, M.; Weyer, S. Cu isotope fractionation during reduction processes in aqueous systems: evidences from electrochemical deposition. *Contrib. Mineral. Petrol.* **2019**, *174* (4), 37.
(36) Mathur, R.; Falck, H.; Belogub, E.; Milton, J.; Wilson, M.; Rose, A.; Powell, W. Origins of Chalcocite Defined by Copper Isotope Values. *Geofluids* **2018**, *2018*, 1−9.
(37) Zavina-James, N. A. V.; Zerkle, A. L.; Steele, R. C. J.; Warke, M. R.; Izon, G.; Savage, P. S. A copper isotope investigation of methane cycling in Late Archaean sediments. *Precambrian Res.* **2021**, *362*, 106267.
(38) Sherman, D. M.; Little, S. H. Isotopic disequilibrium of Cu in marine ferromanganese crusts: Evidence from ab initio predictions of Cu isotope fractionation on sorption to birnessite. *Earth Planet. Sci. Lett.* **2020**, *549*, 116540.
(39) Moynier, F.; Vance, D.; Fujii, T.; Savage, P. The Isotope Geochemistry of Zinc and Copper. *Rev. Mineral. Geochem.* **2017**, *82* (1), 543−600.
(40) Ryan, B. M.; Kirby, J. K.; Degryse, F.; Scheiderich, K.; McLaughlin, M. J. Copper Isotope Fractionation during Equilibration with Natural and Synthetic Ligands. *Environ. Sci. Technol.* **2014**, *48* (15), 8620−8626.
(41) Pokrovski, G. S.; Borisova, A. Y.; Harrichoury, J. C. The effect of sulfur on vapor-liquid fractionation of metals in hydrothermal systems. *Earth Planet. Sci. Lett.* **2008**, *266* (3−4), 345−362.
(42) Grybos, M.; Davranche, M.; Gruau, G.; Petitjean, P. Is trace metal release in wetland soils controlled by organic matter mobility or Fe-oxyhydroxides reduction? *J. Colloid Interface Sci.* **2007**, *314* (2), 490−501.
(43) Little, S. H.; Sherman, D. M.; Vance, D.; Hein, J. R. Molecular controls on Cu and Zn isotopic fractionation in Fe-Mn crusts. *Earth Planet. Sci. Lett.* **2014**, *396*, 213−222.
(44) Moffett, J. W.; Dupont, C. Cu complexation by organic ligands in the sub-arctic NW Pacific and Bering Sea. *Deep Sea Res., Part I* **2007**, *54* (4), 586−595.
(45) Coale, K. H.; Bruland, K. W. Copper complexation in the Northeast Pacific. *Limnol. Oceanogr.* **1988**, *33* (5), 1084−1101.
(46) Bigalke, M.; Weyer, S.; Kobza, J.; Wilcke, W. Stable Cu and Zn isotope ratios as tracers of sources and transport of Cu and Zn in contaminated soil. *Geochim. Cosmochim. Acta* **2010**, *74* (23), 6801−6813.
(47) Fujii, T.; Moynier, F.; Abe, M.; Nemoto, K.; Albarède, F. Copper isotope fractionation between aqueous compounds relevant to low temperature geochemistry and biology. *Geochim. Cosmochim. Acta* **2013**, *110*, 29−44.
(48) Sherman, D. M. Equilibrium isotopic fractionation of copper during oxidation/reduction, aqueous complexation and ore-forming processes: Predictions from hybrid density functional theory. *Geochim. Cosmochim. Acta* **2013**, *118*, 85−97.
(49) Bigalke, M.; Weyer, S.; Wilcke, W. Copper Isotope Fractionation during Complexation with Insolubilized Humic Acid. *Environ. Sci. Technol.* **2010**, *44* (14), 5496−5502.
(50) Shie, J. L.; Chen, Y. H.; Chang, C. Y.; Lin, J. P.; Lee, D. J.; Wu, C. H. Thermal Pyrolysis of Poly(vinyl alcohol) and Its Major Products. *Energy Fuels* **2002**, *16* (1), 109−118.
(51) Neumann, J. P.; Zhong, T.; Chang, Y. A. The Cu-O (Copper-Oxygen) system. *Bull. Alloy Phase Diagrams* **1984**, *5*, 136−140.
(52) Palmer, D. A. Solubility measurements of crystalline Cu2O in aqueous solution as a function of temperature and pH. *J. Solution Chem.* **2011**, *40* (6), 1067−1093.
(53) Mesmer, R. E.; Patterson, C. S.; Busey, R. H.; Holmes, H. F. Ionization of acetic acid in aq. sodium chloride media: a potentiometric study to 573K and 130 bar. *J. Phys. Chem.* **1989**, *93* (21), 7483−7490.
(54) Drummond, S. E.; Palmer, D. A. Thermal decarboxylation of acetate. Part II. Boundary conditions for the role of acetate in the primary migration of natural gas and the transportation of metals in hydrothermal systems. *Geochim. Cosmochim. Acta* **1986**, *50* (5), 825−833.
(55) Dickson, F. W.; Blount, C. W.; Tunell, G. Use of hydrothermal solution equipment to determine the solubility of anhydrite in water from 100 degrees C to 275 degrees C and from 1 bar to 1000 bars pressure. *Am. J. Sci.* **1963**, *261* (1), 61−78.
(56) Seyfried, W. E.; Gordon, P. C.; Dickson, F. W. A new reaction cell for hydrothermal solution equipment. *Am. Mineral.* **1979**, *64*, 646−649.
(57) Qi, D.; Zhang, C.; Lazarov, M. Cu isotope fractionation between Cu-bearing phases and hydrothermal fluids: insights from ex situ and in situ experiments. *Am. Mineral.* **2023**. In press.
(58) Pouchou, J. L.; Pichoir, F. Quantitative analysis of homogeneous or stratified microvolumes applying the model PAP. *Electron Probe Quant.* **1991**, 31−75.
(59) Roebbert, Y.; Rabe, K.; Lazarov, M.; Schuth, S.; Schippers, A.; Dold, B.; Weyer, S. Fractionation of Fe and Cu isotopes in acid mine tailings: Modification and application of a sequential extraction method. *Chem. Geol.* **2018**, *493*, 67−79.
(60) Horn, I.; von Blanckenburg, F.; Schoenberg, R.; Steinhoefel, G.; Markl, G. In situ iron isotope ratio determination using UV-femtosecond laser ablation with application to hydrothermal ore formation processes. *Geochim. Cosmochim. Acta* **2006**, *70* (14), 3677−3688.
(61) Lazarov, M.; Horn, I. Matrix and energy effects during in-situ determination of Cu isotope ratios by ultraviolet-femtosecond laser ablation multicollector inductively coupled plasma mass spectrometry. *Spectrochim. Acta, Part B* **2015**, *111*, 64−73.
(62) Helten, O.; Ostertag-Henning, C.; Bach, W.; Hinrichs, K. U. Generation and decomposition of low-molecular-weight organic acids in hydrous pyrolysis experiments with Opalinus Clay rock. *Org. Geochem.* **2022**, *172*, 104481.
(63) Ni, P.; Macris, C. A.; Darling, E. A.; Shahar, A. Evaporation-induced copper isotope fractionation: Insights from laser levitation experiments. *Geochim. Cosmochim. Acta* **2021**, *298*, 131−148.
(64) Moore, W. J.; Selikson, B. The Diffusion of Copper in Cuprous Oxide. *J. Chem. Phys.* **1951**, *19* (12), 1539−1543.
(65) Rebane, J.; Yakovlev, N.; Chicherin, D.; Tretyakov, Y.; Leonyuk, L. I.; Yakunin, V. G. An experimental study of copper self-diffusion in CuO, Y 2 Cu 2 O 5 and YBa 2 Cu 3 O 7-x by secondary neutral mass spectrometry. *J. Mater. Chem.* **1997**, *7* (10), 2085−2089.
(66) Wells, A. F. XXV. Crystal habit and internal structure II. *London, Edinburgh Dublin Phil. Mag. J. Sci.* **1946**, *37* (267), 217−236.
(67) Lai, F.; Liu, L.; Cao, W. Complexation of copper in acetate-rich low-temperature hydrothermal fluids: Evidence from ab initio molecular dynamics simulations. *Chem. Geol.* **2018**, *476*, 100−118.
(68) Sullivan, J. D.; Oldright, G. L. *The Dissolution of Cuprite in Sulphuric Acid and in Ferric Sulphate Solution*; US Department of Commerce, Bureau of Mines, 1929.
(69) Wadsworth, M. E.; Wadia, D. R. Reaction rate study of the dissolution of cuprite in sulphuric acid. *JOM* **1955**, *7*, 755−759.

(70) Park, I.; Yoo, K.; Alorro, R. D.; Kim, M.; Kim, S. Leaching of copper from cuprous oxide in aerated sulfuric acid. *Mater. Trans.* **2017**, *58* (10), 1500−1504.
(71) Majima, H.; Awakura, Y.; Enami, K.; Ueshima, H.; Hirato, T. Kinetic study of the dissolution of cuprite in oxyacid solutions. *Metall. Trans. B* **1989**, *20* (5), 573−580.
(72) Thornber, M. R. Supergene alteration of sulphides: VII. Distribution of elements during the gossan-forming process. *Chem. Geol.* **1985**, *53* (3−4), 279−301.
(73) Bandura, A. V.; Lvov, S. N. The ionization constant of water over wide ranges of temperature and density. *J. Phys. Chem. Ref. Data* **2006**, *35* (1), 15−30.
(74) Bornhorst, T.; Mathur, R. Copper Isotope Constraints on the Genesis of the Keweenaw Peninsula Native Copper District, Michigan, USA. *Minerals* **2017**, *7*, 185.
(75) Cornwall, H. R. Ilmenite, magnetite, hematite, and copper in lavas of the Keweenawan series [Michigan]. *Econ. Geol.* **1951**, *46* (1), 51−67.
(76) Ustunisik, G.; Kilinc, A.; Nielsen, R. L. New insights into the processes controlling compositional zoning in plagioclase. *Lithos* **2014**, *200*−*201*, 80−93.
(77) Adegoke, I. A.; Xia, F.; Deditius, A. P.; Pearce, M. A.; Roberts, M. P.; Brugger, J. A new mode of mineral replacement reactions involving the synergy between fluid-induced solid-state diffusion and dissolution-reprecipitation: A case study of the replacement of bornite by copper sulfides. *Geochim. Cosmochim. Acta* **2022**, *330*, 165−190.
(78) Chaudhari, A.; Brugger, J.; Ram, R.; Chowdhury, P.; Etschmann, B.; Guagliardo, P.; Xia, F.; Pring, A.; Gervinskas, G.; Liu, A.; et al. Synchronous solid-state diffusion, dissolution-reprecipitation, and recrystallization leading to isotopic resetting: insights from chalcopyrite replacement by copper sulfides. *Geochim. Cosmochim. Acta* **2022**, *331*, 48−68.
(79) Seward, T. M. The stability of chloride complexes of Silver in hydrothermal solutions up to 350°C. *Geochim. Cosmochim. Acta* **1976**, *40* (11), 1329−1341.
(80) Qi, D. Isotopic and Elemental Distribution of Copper between Cu-Bearing Minerals and Aqueous Fluids: Implications of an Experimental Study. Ph.D. Thesis, Institutionelles Repositorium der Leibniz Universität Hannover, Hannover, 2019.
(81) Dekov, V. M.; Rouxel, O.; Asael, D.; Hålenius, U.; Munnik, F. Native Cu from the oceanic crust: Isotopic insights into native metal origin. *Chem. Geol.* **2013**, *359*, 136−149.
(82) Azaraien, H.; Shahabpour, J.; Aminzadeh, B. Metallogenesis of the sediment-hosted stratiform Cu deposits of the Ravar Copper Belt (RCB), Central Iran. *Ore Geol. Rev.* **2017**, *81*, 369−395.
(83) Sun, Y. Z.; Püttmann, W. The role of organic matter during copper enrichment in Kupferschiefer from the Sangerhausen basin, Germany. *Org. Geochem.* **2000**, *31* (11), 1143−1161.
(84) Cox, D. P.; Lindsey, D. A.; Singer, D. A.; Diggles, M. F. *Sediment-Hosted Copper Deposits of the World: Deposit Models and Database*; Citeseer, 2007.
(85) Brown, A. C. A process-based approach to estimating the copper derived from red beds in the sediment-hosted stratiform copper deposit model. *Econ. Geol.* **2009**, *104* (6), 857−868.
(86) Hitzman, M.; Kirkham, R.; Broughton, D.; Thorson, J.; Selley, D. The sediment-hosted stratiform copper ore system. *Econ. Geol.* **2005**, *100*, 609−642.
(87) Putnis, A. Mineral Replacement Reactions. *Rev. Mineral. Geochem.* **2009**, *70* (1), 87−124.
(88) Markl, G.; Lahaye, Y.; Schwinn, G. Copper isotopes as monitors of redox processes in hydrothermal mineralization. *Geochim. Cosmochim. Acta* **2006**, *70* (16), 4215−4228.
(89) Larson, P. B.; Maher, K.; Ramos, F. C.; Chang, Z.; Gaspar, M.; Meinert, L. D. Copper isotope ratios in magmatic and hydrothermal ore-forming environments. *Chem. Geol.* **2003**, *201*, 337−350.
(90) Larsson, P. O.; Andersson, A.; Wallenberg, L. R.; Svensson, B. Combustion of CO and Toluene; Characterisation of Copper Oxide Supported on Titania and Activity Comparisons with Supported Cobalt, Iron, and Manganese Oxide. *J. Catal.* **1996**, *163* (2), 279−293.
(91) Hong, Z.; Cao, Y.; Deng, J. A convenient alcohothermal approach for low temperature synthesis of CuO nanoparticles. *Mater. Lett.* **2002**, *52* (1−2), 34−38.
(92) Kida, T.; Oka, T.; Nagano, M.; Ishiwata, Y.; Zheng, X. G. Synthesis and application of stable copper oxide nanoparticle suspensions for nanoparticulate film fabrication. *J. Am. Ceram. Soc.* **2007**, *90* (1), 107−110.
(93) Sahooli, M.; Sabbaghi, S.; Saboori, R. Synthesis and characterization of mono sized CuO nanoparticles. *Mater. Lett.* **2012**, *81*, 169−172.
(94) Lin, Z.; Han, D.; Li, S. Study on thermal decomposition of copper(II) acetate monohydrate in air. *J. Therm. Anal. Calorim.* **2012**, *107* (2), 471−475.
(95) Bellini, J. V.; Machado, R.; Morelli, M. R.; Kiminami, R. Thermal, Structural and Morphological Characterisation of Freeze-dried Copper(II) Acetate Monohydrate and its Solid Decomposition Products. *Mater. Res.* **2002**, *5* (4), 453−457.
(96) Oral, A. Y.; Menşur, E.; Aslan, M. H.; Başaran, E. The preparation of copper(II) oxide thin films and the study of their microstructures and optical properties. *Mater. Chem. Phys.* **2004**, *83* (1), 140−144.

https://doi.org/10.1021/acsearthspacechem.3c00254
ACS Earth Space Chem. 2024, 8, 499−519